Stability and transition of a supersonic laminar boundary layer on an insulated flat plate

By JOHN LAUFER AND THOMAS VREBALOVICH
Jet Propulsion Laboratory, California Institute of Technology, Pasadena, California

(Received 9 May 1960)

Self-excited oscillations have been discovered experimentally in a supersonic laminar boundary layer along a flat plate. By the use of appropriate measuring techniques, the damping and amplification of the oscillations are studied and the stability limits determined at free-stream Mach numbers 1·6 and 2·2. The wave-like nature of the oscillations is demonstrated and their wave velocities are measured using a specially designed 'disturbance generator'. It is shown empirically that the stability limits expressed in terms of the boundary-layer-thickness Reynolds number are independent of the Mach number and dependent only on the oscillation frequency. The main effect of compressibility is an increase in wave velocity with Mach number. This has the consequence that the disturbances, although possessing the same dimensionless amplification coefficient as in the incompressible case, have less time (per unit distance) to grow in amplitude. Thus, the adiabatic compressible boundary layer is shown to be more stable than the incompressible one. In general, the experiments confirm the basic assumptions and predictions of the existing stability theory and also suggest the desirability of improvement in the theory in certain phases of the problem. Finally, on the basis of these results a rough estimate of the transition Reynolds number is made in the compressible flow range.

1. Introduction

The transition of a boundary layer from a laminar to a turbulent state is one of the outstanding unsolved problems in fluid mechanics. Its practical importance is especially recognized in supersonic flows, where the accompanying aerodynamic heating effects become an essential design consideration.

Today it is a well-accepted fact that in incompressible flows transition is the result of not one but of several instability mechanisms (Dryden 1955; Morkovin 1958). The first stage of the process is the so-called instability with respect to small disturbances (provided the free steam is void of large disturbances). This instability provides the triggering mechanism for the whole transition process and therefore must be considered very important. There are many indications that in compressible flows the transition phenomenon is basically the same. The present investigation was therefore undertaken with the belief that the study of the first stage of transition in the compressible boundary layer, the instability with respect to small disturbances, should result in valuable information.

When the historical development of the stability problem in the incompressible

laminar boundary layer is considered, it is surprising to note that despite the great interest of theoretical researchers and the great practical importance of the problem, very few basic stability experiments were carried out. The comparatively slow progress and the strong controversies in the 1930's were mainly the result of this lack of basic experimental work. After all, fourteen years elapsed between 1929, when Tollmien (1929) first published his small-disturbance theory for the boundary layer, and 1943, when the experiments of Schubauer & Skramstad (1948) fully confirmed the theory. During this period the theory was exposed to strong criticism, not only because of its lack of mathematical rigour, but also because of its underlying physical model for the transition process. Specifically, the theory was attacked because the connexion between the small-disturbance instability and transition was not understood at that time, and the linearized two-dimensional theory was considered too great an oversimplification to describe adequately the strongly non-linear transition process. Furthermore, the self-excited boundary-layer oscillations, the most striking prediction of the theory, had not yet been observed. Obviously, only direct experiments could and did satisfy such criticism. The measurements of Schubauer & Skramstad demonstrated not only the existence of the instability waves, but also the fact that the behaviour of these waves agrees quantitatively with the theoretical predictions. These experiments were followed by a few similarly basic ones: Liepmann (1943) applied the technique to boundary layers on curved walls; Bennett (1953) considered the effect of increased free-stream turbulence level on stability; and, finally, Wortmann (1955) studied the stability problem using a completely different experimental method. It is believed that as a result of these experiments and of the theoretical studies, especially those of Lin (1945), who answered the remaining mathematical questions, the first stage of transition in the incompressible boundary layer is well understood.

If attention is turned now to the stability problem in the compressible boundary layer, the lack of basic experimental work again becomes evident. After 1946, when the pioneering theoretical work of Lees & Lin (1946) extended the small-disturbance stability theory to flows at low supersonic Mach numbers, no pertinent experiments were reported in the literature for more than ten years. In contrast to the incompressible theory, however, the theoretical work gained ready acceptance; in fact, it was even applied to problems outside the immediate scope of the theory. Lees & Lin have clearly indicated that their work is restricted to flows at low Mach numbers (below approximately 1·5), where the wave velocities are small compared with the free-stream velocity and where the temperature fluctuations can be neglected in the relation for the characteristic values of the problem. These limitations were partially removed by Dunn & Lin (1955), who also included three-dimensional disturbances in their theory. Any further extension of the theory to high Mach numbers, however, would become exceedingly difficult because of some of the inherent assumptions in the formulation of the theory. Neglect of disturbances that are supersonic relative to the free stream, for instance, would have to be justified. Undoubtedly, measurements examining such questions would be of great value.

The available experiments, however, do not deal with this basic problem, but

with the study of the transition 'point' of a compressible boundary layer in the light of the stability theories. Although, in principle, strong objections may be raised against such direct comparisons, some qualitative results have been obtained. It has been shown in several instances that surface cooling increases the transition Reynolds number, which is consistent with Lees's prediction of increased stability with cooling (e.g. Lees 1947). Furthermore, various investigators have reported that with increasing Mach number it becomes more difficult to trip the boundary layer, indicating in a loose sense that the layer becomes more stable at larger Mach numbers, which is again consistent with Lees's (1952) calculations of decreasing amplification rates.

At the time the present work was initiated, no experiments which directly concerned the first stage of transition (experiments analogous to those of Schubauer & Skramsted in incompressible flows) existed. This situation derived from several serious difficulties. It is well known from experience in incompressible flows that a suitable experimental environment is of vital importance. Not only the mean velocity and pressure gradients in the wind tunnel, but the tunnel turbulence level, as well, must be minimized. Supersonic free-stream turbulence is not yet well understood. Also, mechanical and electronic instrumentation can present a major difficulty. In the measurement of small-amplitude flow fluctuations, it is obvious that mechanical vibrations in the traversing mechanisms, probes, and flat plates must be largely eliminated. Finally, the hot-wire technique must be developed and adapted so that measurements up to 100,000 c/s can be carried out and interpreted correctly.

The experiments presented here succeeded to a large extent in overcoming these difficulties. By a careful and detailed examination of the free-stream fluctuations in the wind tunnel, a Mach number range in which the stability measurements could be accepted with confidence was chosen. The mechanical instrumentation was designed in such a way that any vibration or flow disturbance induced by the system could be immediately detected and corrected. Finally, the hot-wire technique and accompanying instrumentation were developed to the extent that they were not the major limiting factors in determining the scope of the experiments.

Under these circumstances the investigation at the Jet Propulsion Laboratory succeeded in accomplishing the following:

(1) The existence of self-excited oscillations in a supersonic boundary layer was shown experimentally.

(2) A detailed study of the behaviour of these oscillations was made, and the results were compared with theoretical predictions.

(3) Some of the differences between the stability of the incompressible boundary layer and the stability of the supersonic boundary layer were further brought to focus.

Some early results of this work are described elsewhere (Laufer 1956; Laufer & Vrebalovich 1957). Also, parallel with the present investigation, Demetriades (1958, 1960) obtained some interesting results on the stability problem in the hypersonic tunnel of the California Institute of Technology at Mach number 5·8 using techniques similar to those described here.

2. Experimental equipment

2.1. *Wind tunnel*

Most of the measurements were carried out in the Jet Propulsion Laboratory 18 × 20 in. supersonic wind tunnel; some of the initial data were obtained in the 12 × 12 in. wind tunnel. The Mach number in the working section of the larger tunnel was continuously variable from 1·3 to 5·0. The distribution of the static pressure in the test section was uniform to within 2 % along the centre-line and 5 % six inches below and above the centre-line in the whole Mach number range. Such a uniform mean flow field served to great advantage in these experiments.

Considerable time and effort were spent to reduce the turbulence level in the supply section. Figure 1 shows a portion of the tunnel circuit. The first two screens shown in the short entrance diffuser were installed in order to prevent local flow separation. At the entrance of the 8 ft. diameter stagnation chamber, an Airmat paper filter* was stretched across the section to protect the hot wires from fine dust particles. The subsequent six damping screens served to reduce the turbulence level.

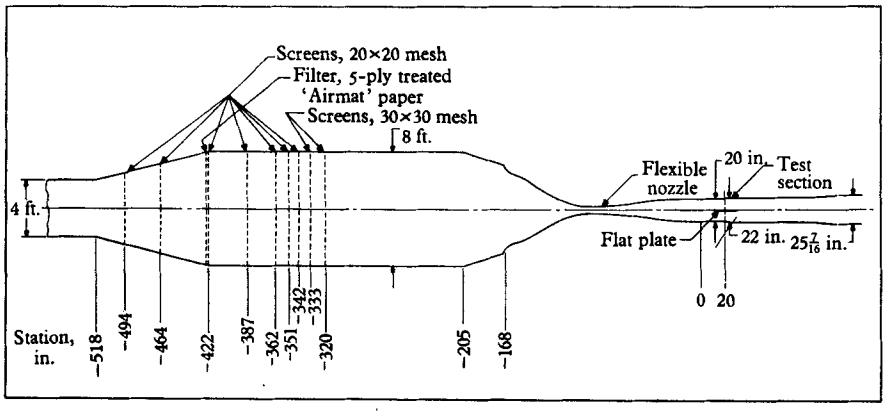

FIGURE 1. Supply section and test section of 18 × 20 in. wind tunnel.

Turbulence-level measurements in the supply section were made approximately 2½ ft. downstream of the last damping screen. The results indicated that the temperature fluctuations were negligibly small and the velocity fluctuations were 1 % of the local mean velocity for all the tunnel pressures and free-stream Mach numbers except for $M_1 \geqslant 4{\cdot}5$, where the level dropped to ½ %. When it is considered that even for the lowest Mach number flow the velocity ratio of the free-stream and supply-section flow is somewhat more than 40 : 1, a velocity fluctuation of less than 0·01 % in the free stream is calculated using Tucker's method (1953). Consequently, the 1 % turbulence level in the supply section was believed to be satisfactory.

Measurements in the supersonic free stream presented much more difficulty. By use of a method proposed by Kovasznay (1953) and Morkovin (1956), the

* Manufactured by American Air Filter, Louisville, Ky.

mass-flow (figure 2) and total-temperature fluctuations could be calculated and were found to increase very rapidly with Mach number. It is also seen in the figure that the fluctuations increase with decreasing tunnel pressure. The results of a detailed study of this problem will be published elsewhere (Laufer 1959) and will therefore not be described. Briefly, the fluctuations found in the free stream are shown to be due to a pure sound field produced by the thick turbulent boundary layers of the tunnel walls. Any reduction of the turbulence level at the higher Mach number flows would involve removing the boundary layers from the tunnel walls, an extremely elaborate and difficult task, or operating the wind tunnel at pressure levels low enough to sustain laminar boundary layers. Unfortunately, because of practical limitations, neither was possible.

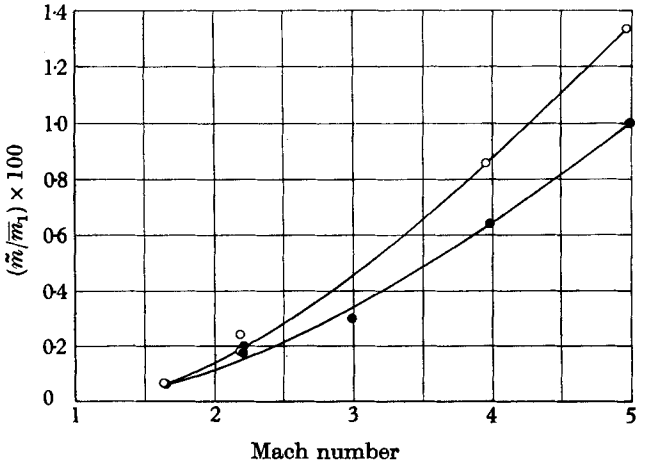

FIGURE 2. Mass-flow fluctuations in test section.
○, Re/in. ~ 90,000; ●, Re/in. ~ 330,000.

From the above considerations it is obvious that any boundary-layer-stability work, in which low free-stream turbulence level is a necessity, is possible only at the lower Mach number flows in this tunnel. The choice of the upper Mach number limit is described in § 5.3.

2.2. *Flat plates*

The experiments were carried out using two different flat plates. For the measurements at $M_1 = 1{\cdot}6$, a $\frac{1}{2}$ in. thick, 25 in. long, plate with a leading edge of 13 degrees was used. For the measurements at higher Mach numbers, a 1 in. thick, 33 in. long, plate with a leading-edge angle of 24 degrees was provided. Both plates were ground and lapped; the leading-edge radii were less than 0·001 in.

2.3. *Traversing mechanisms*

Most of the data were obtained with the hot-wire probe attached to a servo-controlled carriage and traversing mechanism (figures 3 and 4). The mechanical details are described elsewhere (Laufer & Vrebalovich 1958).

2.4. *Hot-wire probes*

In all of the experiments described, the hot wires were 90% platinum–10% rhodium and were 0·00005 or 0·0001 in. in diameter with nominal lengths of 0·015 or 0·020 in., respectively. The hot-wire probe (figure 5, plate 1) is mounted in the carriage as shown in figure 4.

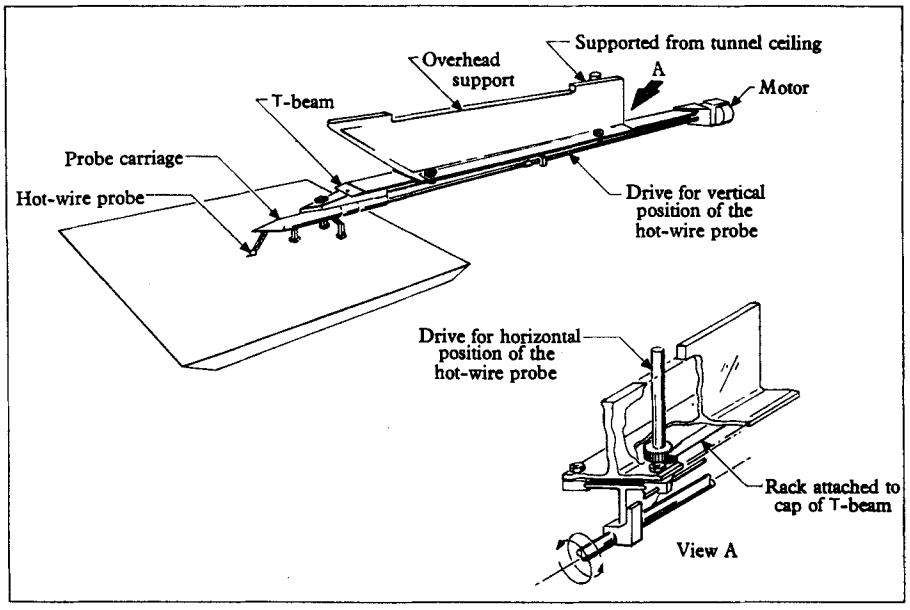

FIGURE 3. Diagram of x-traversing mechanism.

2.5. *Disturbance generator*

The basic problem was to generate the disturbances in the frequency range of 5000 to 50,000 c/s without affecting the normal boundary-layer growth and the flow field. Several different methods were attempted in order to produce single-frequency disturbances near the leading edge of the flat plate.

The disturbance generator finally adopted was essentially a high-speed valve. This opened and closed a narrow slit in the surface of the flat plate to allow periodic air pulses of any desired strength and frequency to disturb the boundary layer on the surface of the plate. The main part of this generator was a hollow cylinder (figure 6) 0·3 in. in diameter and 3·0 in. long (1·5 in. long for the 1 in. thick plate), with 40 slots, 0·01 in. wide, milled parallel to its axis (figure 7, plate 2). A slot (figure 6) 0·003 in. wide and 3 in. long was milled near the plate centre-line in the surface of the plate along the axis of the cylinder 1·7 in. (0·8 in. for the 1 in. thick plate) from the leading edge. The cylinder was connected to the variable-speed motor by means of gears, a long shaft in the plate, a high-speed grinder spindle, and a timing belt and pulleys. This arrangement can be seen in figure 8 (plate 3). The maximum rpm of the motor was 5000; this corresponded to the 90,000 rpm of the cylinder.

The chamber that surrounded the slotted cylinder was sealed by a cover plate and by a Van de Graaff type of seal around the shaft (Strong 1938). Air was allowed to enter the chamber through a porous plug in order to obtain uniform flow through the slit along its 3 in. length (figure 7, plate 2). The flow rate (i.e. the disturbance amplitude) was regulated by a needle valve. The generator frequency was monitored by the arrangement seen in figure 7 (plate 2). A light source and

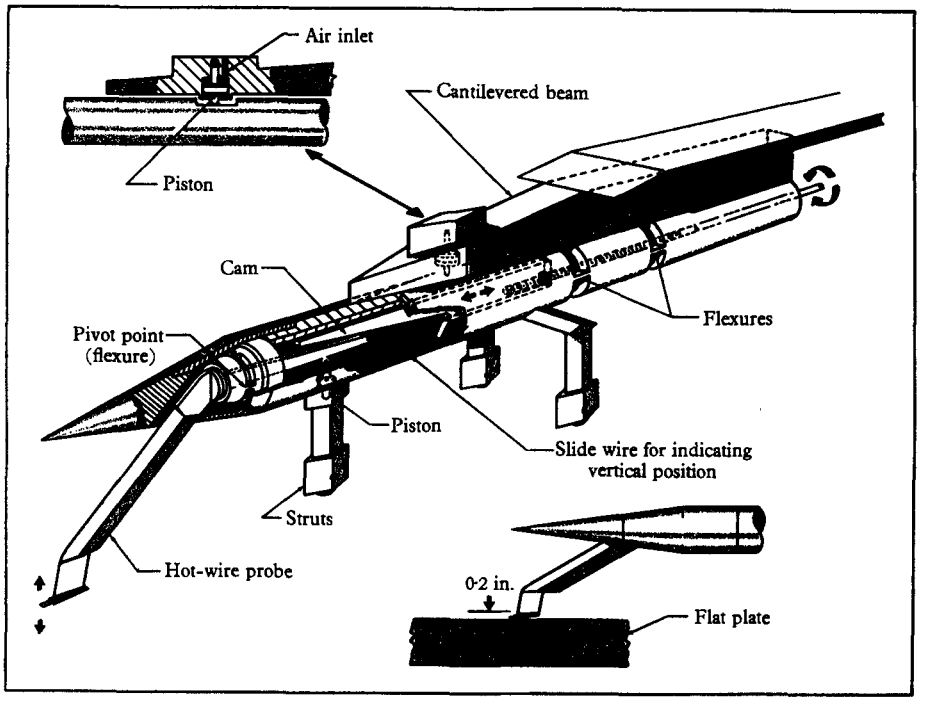

FIGURE 4. Hot-wire carriage and y-traversing mechanism.

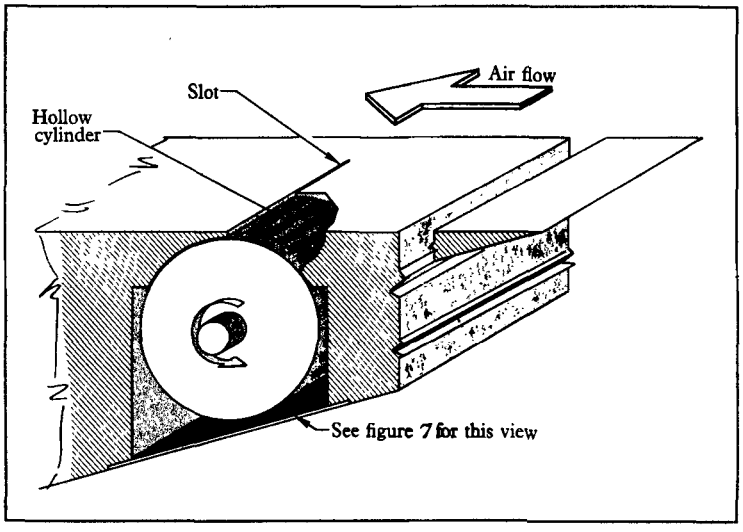

FIGURE 6. Schematic diagram of the disturbance generator.

photocell were placed so that the reflected light from the rotating cylinder struck the photocell. Each time one of the cylinder slats passed the light path a reflexion occurred which was recorded by the photocell. Thus, the output of the photocell gave the proper reference frequency.

2.6. *Hot-wire set, auxiliary equipment*

Hot-wire amplifier. The design requirements of the hot-wire equipment used for fluctuation measurements in supersonic flows have been described in detail by Kovasznay (1954). The high frequencies that are expected in supersonic flow fields necessitate an amplifier with a frequency response of several hundred kilocycles. Low-noise input circuitry is critical in such an amplifier, especially because of the greater frequency bandwidth and low level of the fluctuations expected. The commercially available Shapiro–Edwards Model 50 B constant-current hot-wire set (Shapiro and Edwards, South Pasadena, California) satisfies these requirements and was used throughout the experiment.

Wave analysers. Several different harmonic wave analysers were used to determine the power spectrum of the hot-wire signals. A Panoramic SB 7a ultrasonic harmonic wave analyser (Panoramic Radio Products, Inc., Mt Vernon, N.Y.), which exhibited the spectrum of the hot-wire signal from 1 to 300 kc on an internal oscilloscope, was very useful in quickly showing if there were extraneous oscillations in the signal. Sharp peaks in the spectrum distribution observed on the analyser indicated hot-wire or probe vibrations, possible flat-plate vibrations, or oscillations in electronic equipment; and remedial measures could be taken immediately.

Quantitative power-spectrum measurements were obtained with two different harmonic wave analysers. These instruments were also used as very narrow band-pass filters in order that the growth and decay of the energy in a narrow frequency band of the disturbance could be observed. The low-frequency range of the spectrum was covered by a Hewlett-Packard Model 300 A harmonic wave analyser (Hewlett-Packard Co., Palo Alto, California) with a frequency range of 30–16,000 c/s and a variable effective bandwith of 10 to 45 c/s. The high range of frequencies was detected by a Sierra Model 104 carrier-frequency voltmeter (Sierra Electronic Corp., Menlo Park, California) with a frequency range from 3 to 150 kc and a bandwith of 600 c/s.

The output circuitry of both analysers was modified to enable the installation of a vacuum thermocouple which would give an output thermocouple voltage proportional to the mean square of the output signal of the analyser. The method for plotting spectra will be described in detail in § 4.1.

Plotting table. Power spectra and the growth and decay of disturbances in the boundary layer were plotted on an Electronics Associates Variplotter (Electronic Associates, Inc., Long Branch, N.J.).

3. Theoretical considerations

It is outside the scope of this paper to discuss the theory of compressible-boundary-layer stability; that subject is adequately covered in the literature (Lees & Lin 1946; Dunn & Lin 1955). Instead, attention is focused on the under-

lying assumptions of the theory and on its predictions, so that they may be examined in the light of the experiments.

3.1. *Basic assumptions of the stability theory*

Under consideration are the general equations of motion of an ideal, viscous, heat-conducting, compressible fluid in which perturbations are introduced about a steady-state solution in the form

$$Q(x, y, z, t) = \bar{Q}(x, y, z) + Q'(x, y, z, t).$$

Thus, any quantity Q is decomposed into two parts: a time-averaged mean value and a time-dependent perturbation.

Assumption 1. It is assumed now that

$$\frac{Q'}{\bar{Q}} \ll 1,$$

so that second-order interactions between perturbations can be neglected. As a result of this assumption the equations become linear and can be handled by conventional methods. The theory considers now the flow over a flat plate and makes additional assumptions.

Assumption 2. The usual boundary-layer approximations are introduced. Furthermore, from detailed considerations of orders of magnitude (Dunn & Lin 1955), it is concluded that certain viscous terms in the momentum equations and all the dissipation terms in the energy equation can be neglected provided the Mach number is not very high.

Assumption 3. It is also assumed that the mean flow in the boundary layer can be considered parallel when the boundary-layer stability at a given location is to be obtained. Here again, a high Mach number is the limiting factor for the validity of this assumption (Dunn & Lin 1955).

With these simplifications the structure of the equations allows the perturbations to have the form (see p. 296 for an explanation of the notation)

$$Q' = q\left(\frac{y}{\delta}\right) e^{\beta_i t} e^{i\alpha(x-ct)}, \tag{3.1}$$

where the amplitude function q depends on y/δ only. The more general three-dimensional case is treated by Dunn & Lin (1955).

The simplified equations now take the following form.

Continuity equation:

$$\frac{\partial \rho'}{\partial t} + \bar{u}\frac{\partial \rho'}{\partial x} + v'\frac{\partial \bar{\rho}}{\partial y} + \bar{\rho}\left(\frac{\partial u'}{\partial x} + \frac{\partial v'}{\partial y}\right) = 0. \tag{3.2}$$

Momentum equations:

$$\bar{\rho}\left(\frac{\partial u'}{\partial t} + \bar{u}\frac{\partial u'}{\partial x} + v'\frac{\partial \bar{u}}{\partial y}\right) = -\frac{\partial p'}{\partial x} + \bar{\mu}\frac{\partial^2 u'}{\partial y^2}, \tag{3.3}$$

$$\bar{\rho}\left(\frac{\partial v'}{\partial t} + \bar{u}\frac{\partial v'}{\partial x}\right) = -\frac{\partial p'}{\partial y} + \bar{\mu}\frac{\partial^2 v'}{\partial y^2}. \tag{3.4}$$

Energy equation:

$$\bar{\rho}C_v\left(\frac{\partial T'}{\partial t}+\bar{u}\frac{\partial T'}{\partial x}+v'\frac{\partial \bar{T}}{\partial y}\right)=-\bar{p}\left(\frac{\partial u'}{\partial x}+\frac{\partial v'}{\partial y}\right)+\bar{k}\frac{\partial^2 T'}{\partial y^2}. \tag{3.5}$$

Equation of state:

$$\frac{p'}{\bar{p}}=\frac{\rho'}{\bar{\rho}}+\frac{T'}{\bar{T}}. \tag{3.6}$$

Or, if all the fluctuating quantities are written according to equation (3.1), where f, ϕ, π, r and θ are the amplitude functions of u', v', p', ρ' and T', respectively:

$$i\alpha(\bar{u}-c)r+\phi\frac{\partial\bar{\rho}}{\partial y}+\bar{\rho}\left(i\alpha f+\frac{\partial\phi}{\partial y}\right)=0, \tag{3.7}$$

$$\bar{\rho}\left[i\alpha(\bar{u}-c)f+\phi\frac{\partial\bar{u}}{\partial y}\right]=-\pi i\alpha+\bar{\mu}\frac{\partial^2 f}{\partial y^2}, \tag{3.8}$$

$$\bar{\rho}[i\alpha(\bar{u}-c)\phi]=-\frac{\partial\pi}{\partial y}+\bar{\mu}\frac{\partial^2\phi}{\partial y^2}, \tag{3.9}$$

$$\bar{\rho}C_v\left[i\alpha(\bar{u}-c)\theta+\phi\frac{\partial\bar{T}}{\partial y}\right]=-\bar{p}\left(i\alpha f+\frac{\partial\phi}{\partial y}\right)+\bar{k}\frac{\partial^2\theta}{\partial y^2}, \tag{3.10}$$

$$\frac{\pi}{\bar{p}}=\frac{r}{\bar{\rho}}+\frac{\theta}{\bar{T}}. \tag{3.11}$$

The boundary conditions satisfied by the perturbations at the wall are

$$f(0)=\phi(0)=0,$$

$$a\frac{d\theta}{dy}(0)+b\theta(0)=0,$$

where a and b depend on the frequency of oscillation and the physical properties of the gas and the wall.

On the free-stream side the boundary conditions depend on the nature of the disturbance considered. Here the theory introduces the following assumption.

Assumption 4. Only disturbances that are propagating with subsonic speed with respect to the free stream are considered. It is conjectured that supersonic disturbances do not play an important role in the boundary-layer stability problem. This question has not yet been studied either theoretically or experimentally. From this assumption it follows that, for $y\to\infty$,

$$f,\quad \phi,\quad \text{and}\quad \theta\to 0.$$

With the above six boundary conditions and the sixth-order system of linear differential equations, a characteristic-value problem is defined. The equation relating the eigenvalues may be written formally

$$E(M_1^2, \alpha R_e, \alpha^2, c)=0.$$

The solution of the stability problem is now reduced to solving this relation. In their formulation, Lees & Lin used a method of approximation within

which the above relation and the boundary conditions become independent of the temperature fluctuations. The approximation is based on the following assumption.

Assumption 5. In essence it is required that the critical layer be near the wall. This is valid if the free-stream Mach number is subsonic or slightly supersonic. A consequence of this assumption is that the relation for the characteristic values becomes independent of the temperature fluctuations and the boundary conditions imposed on them. Later Dunn & Lin relaxed this assumption and showed that for higher Mach numbers the role of the temperature fluctuations does become important.

The solution of the above secular equation involves elaborate and complex mathematical arguments, some of which are still not completely settled. However, no new physical assumption is introduced.

3.2. *General results of the theory*

On the basis of these five assumptions the theory leads to the following general conclusions concerning the stability of a compressible boundary layer on an insulated flat plate:

(1) The basic mechanism of stability is the same as that found in the incompressible case.

(2) Three-dimensional disturbances become important at supersonic Mach numbers.

From the relatively few existing numerical calculations (Dunn & Lin 1955; Lees 1947) some interesting insight can also be obtained into the effect of Mach number on the quantitative behaviour of the stability parameters. It is found that with increasing Mach number:

(*a*) The propagation speed increases and the wave-number decreases.

(*b*) The minimum critical Reynolds number diminishes.

(*c*) The maximum amplification ratios also decrease rapidly.

4. Measuring techniques

4.1. *Disturbance amplitude*

In order to measure disturbance amplitudes along the flat plate in a continuous manner, it was of great advantage to maintain the hot wire at a constant sensitivity. It should be remembered that the hot wire is sensitive to a combination of velocity, density and temperature fluctuations and that the relative sensitivities to these fluctuations change if the mean flow field changes. It follows that these sensitivities remain constant as x varies only if for each x-station the wire is placed at y-positions where the mean flow conditions are the same. Since the mean resistance of the hot wire is a sensitive indicator of the mean flow conditions, the voltage unbalance of the hot-wire bridge was used to place the wire automatically at the desired y-position. This was done in the following way. A Brown servo amplifier was connected parallel with the null galvanometer in the hot-wire resistance bridge (figure 9). If the resistance bridge became unbalanced (when, for instance, the wire moved to a slightly different x-position),

the servo amplifier energized a Brown servo motor which in turn caused the hot wire to move in the y-direction until the resistance bridge again was balanced. The y-position of the hot wire was obtained from the contact-point position on the y-slide wire (figure 4). This, together with the Y-axis scale-factor control, provided the y-position signal for one of the Y-axis plotting arms, as shown in figure 9.

The x-position of the hot wire was determined by a slide wire on the T-beam (figure 3). The system for plotting this position was identical with that for the y-position plotting. With this method the spatial position of the wire could be

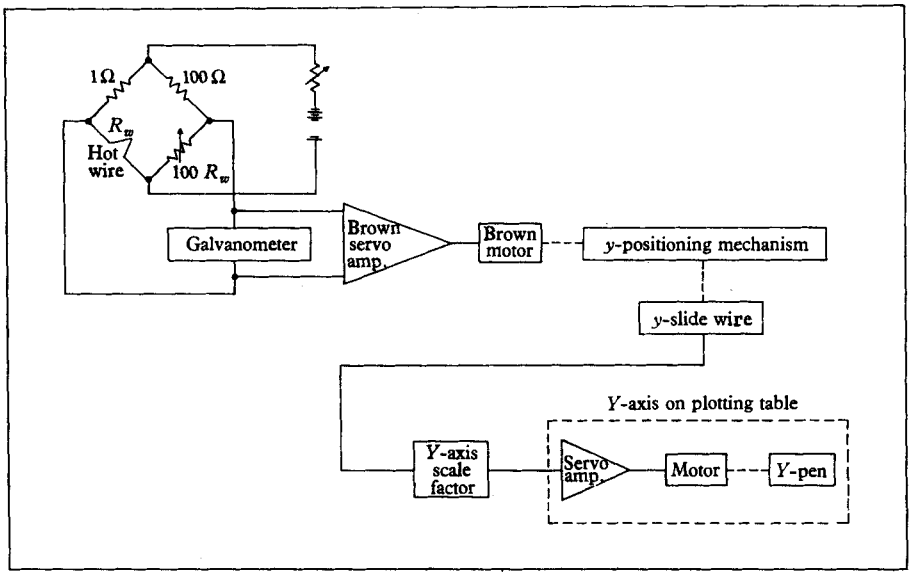

FIGURE 9. Constant y/δ servo system and y-position plotting.

easily followed visually. The wire signal was fed into a wave analyser, the output of which provided the signal $\overline{e_f^2}$ for the second plotting arm of the table. The y-positions of the hot wire and the mean-square output of the analyser were thus plotted simultaneously against the x-position of the hot wire.

It should be mentioned that the plots $\overline{e_f^2}$ *vs* x obtained in this way could be used directly to calculate the logarithmic derivatives (or amplifications) of the velocity, density, or temperature perturbations. Experimentally, it was found that the mass-flow and total-temperature fluctuations were anticorrelated and that at a given y/δ the logarithmic derivative of $\overline{e_f^2}$ was independent of hot-wire temperature (i.e. sensitivity). Under these conditions it may be shown, using the hot-wire equation (5.1), that

$$\frac{1}{2\overline{e_f^2}}\frac{d\overline{e_f^2}}{dx} = \frac{1}{\tilde{Q}}\frac{d\tilde{Q}}{dx},$$

where $\tilde{Q}$ is the root mean square of velocity, density, or temperature perturbation.

4.2. *Wave velocity*

The wave velocity c was obtained from phase measurements using the artificially introduced single-frequency disturbances. The technique is briefly described as follows. The signals from the reference source and from the hot wire located at x have the form

$$e'_{\text{ref}} = a \sin \beta t,$$

$$e'_f = b(x) \sin \beta \left(t - \frac{x}{c} \right),$$

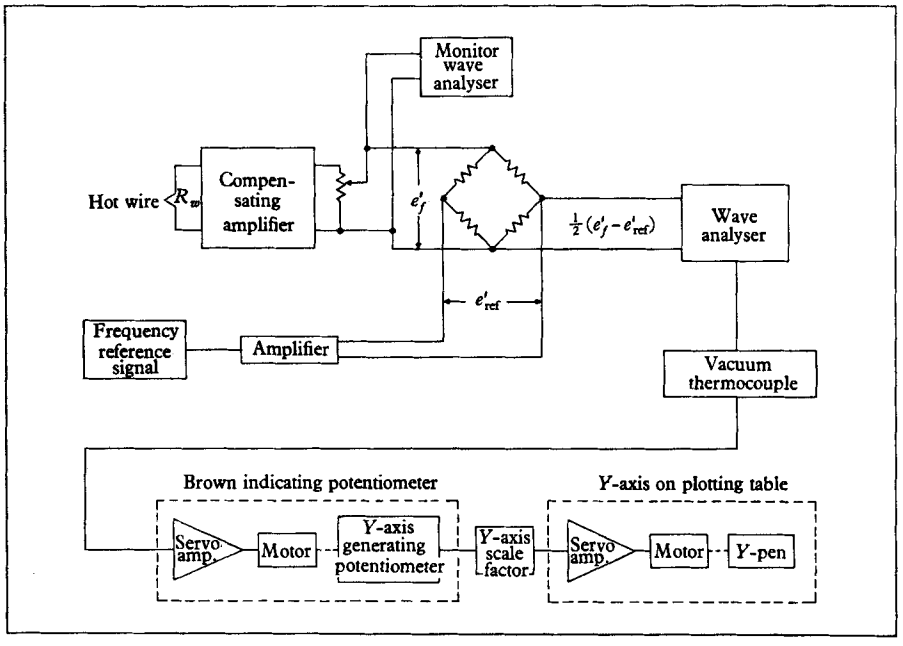

FIGURE 10. Wavelength measurements.

where a is a constant and β is the angular frequency. As the hot wire is moved along the plate the mean-square difference of these two signals can be recorded *vs* x, while $b(x)$ is kept constant. Thus,

$$\overline{(e'_{\text{ref}} - e'_f)^2} = \frac{a^2}{2} + \frac{b^2}{2} - 2ab \overline{\sin \beta t \sin \beta \left(t - \frac{x}{c} \right)}$$

$$= \frac{a^2 + b^2}{2} - ab \cos \beta \frac{x}{c}.$$

It is easily seen that if the mean-square difference goes through a full cycle from position x_1 to x_2, then

$$\frac{\beta}{c}(x_1 - x_2) = 2\pi,$$

or

$$c = \frac{\beta}{2\pi}(x_1 - x_2) = \frac{\beta}{2\pi}\lambda = \lambda f.$$

During the experiment the output of the hot-wire amplifier was fed across two terminals of a balanced bridge and the reference signal was placed across the opposite terminals of the bridge (figure 10). A wave analyser monitored the hot-wire signal in order to keep the amplitude $b(x)$ constant as the hot wire moved along the plate. The mean-square difference of the hot-wire and reference signals was then automatically plotted.

4.3. *Amplitude distribution across the boundary layer*

The hot-wire probe was fixed at a given x-position on the flat plate, and the output and current of the wire were plotted against its y-position. A Brown servo system kept the heated-wire resistance constant as the probe moved through the layer. The y-position of the wire was plotted as the abscissa of the plotting table, and the d.c. current in the wire was one of the two ordinates. The output of the hot-wire amplifier vacuum thermocouple or the wave-analyser vacuum thermocouple was used as the second ordinate on the table. The time constant and sensitivity of the wire changed, of course, as the wire was moved through the layer; these were calculated and the data corrected appropriately. Later, the correct precalibrated time constant was manually set during the measurements.

5. Results and discussion

5.1. *Establishment of a laminar boundary layer*

Before the study of the fluctuations in the boundary layer was undertaken, the mean flow field in the layer was examined. For this reason three types of mean measurements were made: (1) pressure distribution on the plate, (2) rate of boundary-layer growth, and (3) velocity distribution across the layer.

(1) Figure 11 shows the static-pressure distributions along the plate for $M_1 = 1{\cdot}6$ and $M_1 = 2{\cdot}2$ and at tunnel pressures most often used during this investigation. The dashed line indicates the pressure distribution on the centre-line of the empty tunnel. It is seen that in the region of interest the pressure is constant along the plate within 2 %.

(2) The rate of growth of the boundary layer was examined using the method described in § 4.1. By tracing the position of the hot wire as it follows points of constant mean mass flow along the plate, the boundary-layer growth can be easily checked. From boundary-layer similarity considerations the trace, of course, has to be parabolic. This method provided an easy and sensitive means of checking whether or not the measurements were made under the desired conditions. For instance, the trace became non-parabolic if the hot-wire probe was too close to the plate surface and disturbed the flow locally or if a pressure gradient destroyed the similarity because of some exterior condition. All the measurements of disturbance amplitude variations along the plate were accompanied by such traces. A typical example is shown in figure 12. It is to be noted here that near the last inch the trace deviates from the parabola, indicating some irregularity in the flow (nearness of transition).

(3) Measurement of the mean velocity distribution at one station of the plate was also made. This was carried out while artificial disturbances were introduced

in the boundary layer in order to check whether or not the mean flow field had been disturbed by the slight bleeding of air through the slot of the disturbance generator. The accuracy of the mean measurements could have been improved by using a longer and thicker wire; however, fluctuation measurements, which

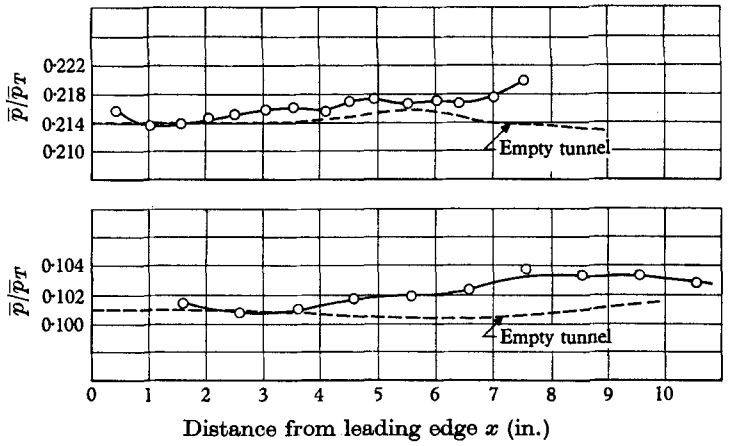

FIGURE 11. Static-pressure distributions along the flat plate and in empty tunnel. Upper figure: $M_1 = 1{\cdot}6$, Re/in. = 180,000. Lower figure: $M_1 = 2{\cdot}2$, Re/in. = 75,000.

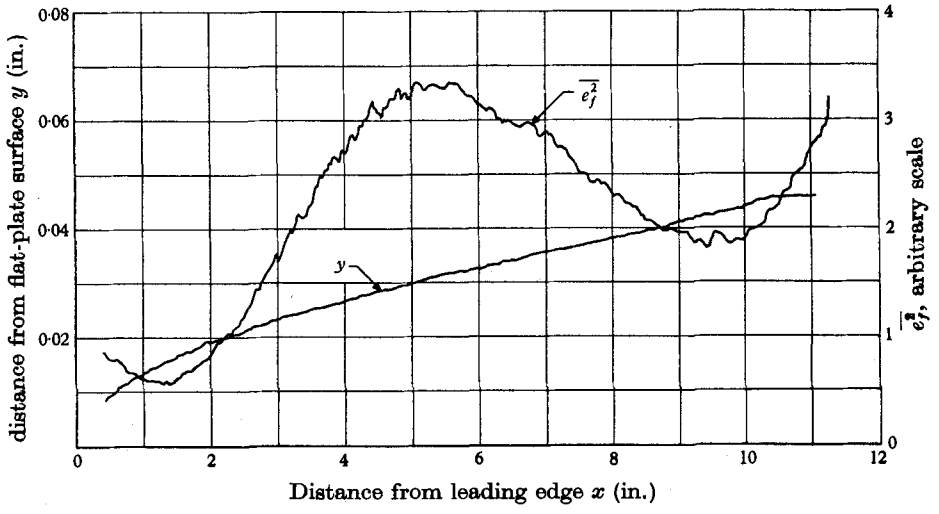

FIGURE 12. Growth of boundary layer and variation of disturbance amplitude along the flat plate. $M_1 = 2{\cdot}2$, Re/in. = 77,000, $f = 23$ kc.

were made simultaneously, limited the wire diameter to small sizes. Figure 13 shows the raw data for the unheated-wire-resistance change in the boundary layer from which the total temperature can be easily calculated. The typical maximum is clearly seen from the trace. Figure 13 also shows the current distribution for one particular temperature loading. From such traces the velocity distribution can be calculated using the method described by Laufer & McClellan

(1956). Also the data provide the necessary information for computing the hot-wire sensitivities. Using these and the mean-square hot-wire output $\overline{e_f^2}$ (figure 14) the various flow fluctuations may be calculated (see § 5.5).

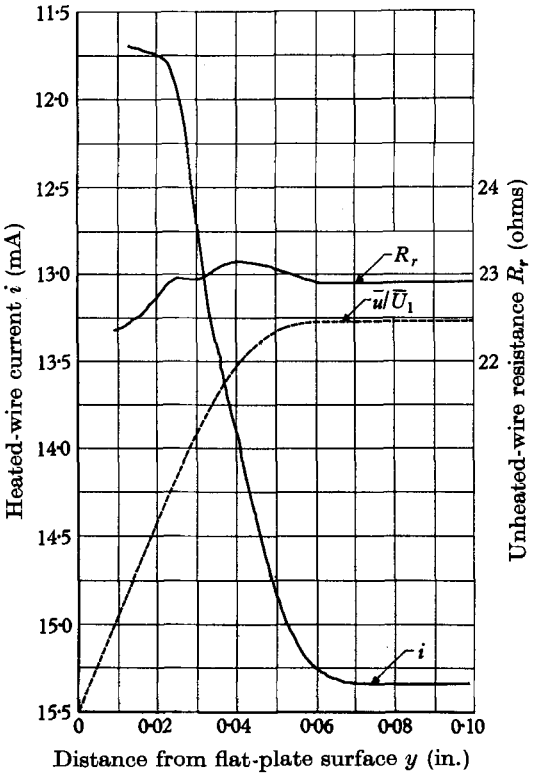

FIGURE 13

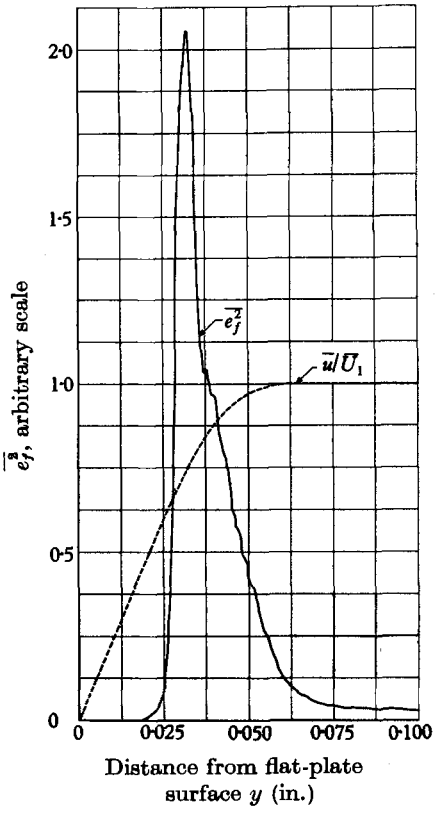

FIGURE 14

FIGURE 13. Unheated-wire resistance and current variation across the boundary layer. $M_1 = 2{\cdot}2$, Re/in. = 77,000, $x = 5$ in., $R_w = 33{\cdot}58\ \Omega$.

FIGURE 14. Mean-square hot-wire voltage across the boundary layer at a fixed frequency. $M_1 = 2{\cdot}2$, Re/in. = 77,000, $x = 5$ in., $f = 23{\cdot}2$ kc.

In figure 15 the solid line is the theoretical velocity distribution calculated by Mack (1958) using the Klunker–McLean method. The agreement between the experiments and theory is seen to be satisfactory. Near the wall (for $M < 1{\cdot}2$) the measurements were not reduced, since here the reduction is more complicated and not reliable. (The heat loss of the wire here is not only a function of the local Reynolds number, but also of the Mach number.) For later reference the calculated Mach number and temperature distribution are also given in figure 16.

5.2. *First indications of instability*

In the stability problem under study here, the existing low-speed experiments and the theory gave many helpful hints as to what to look for and what to observe. However, it was difficult to decide how and where to make the obser-

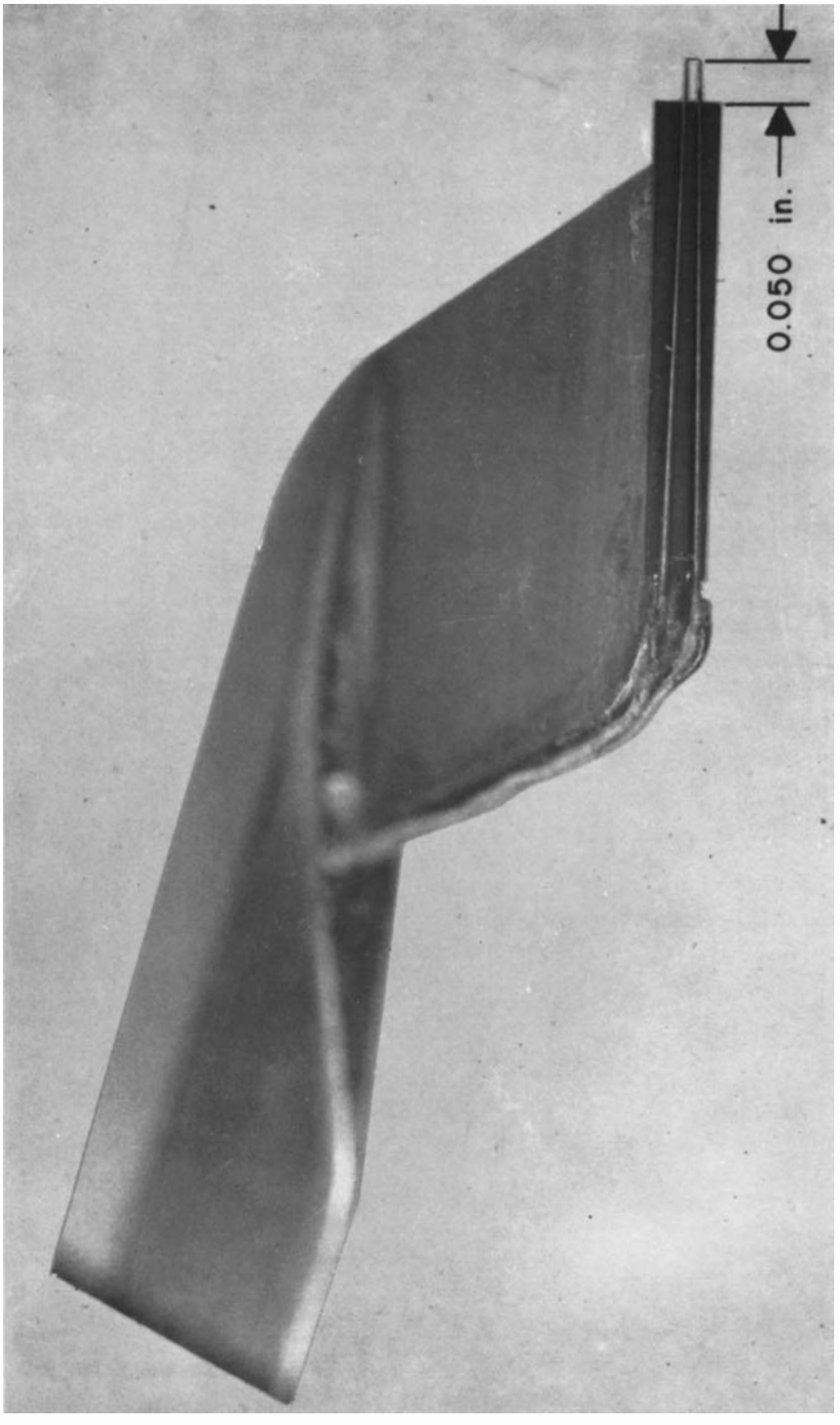

FIGURE 5. Hot-wire probe.

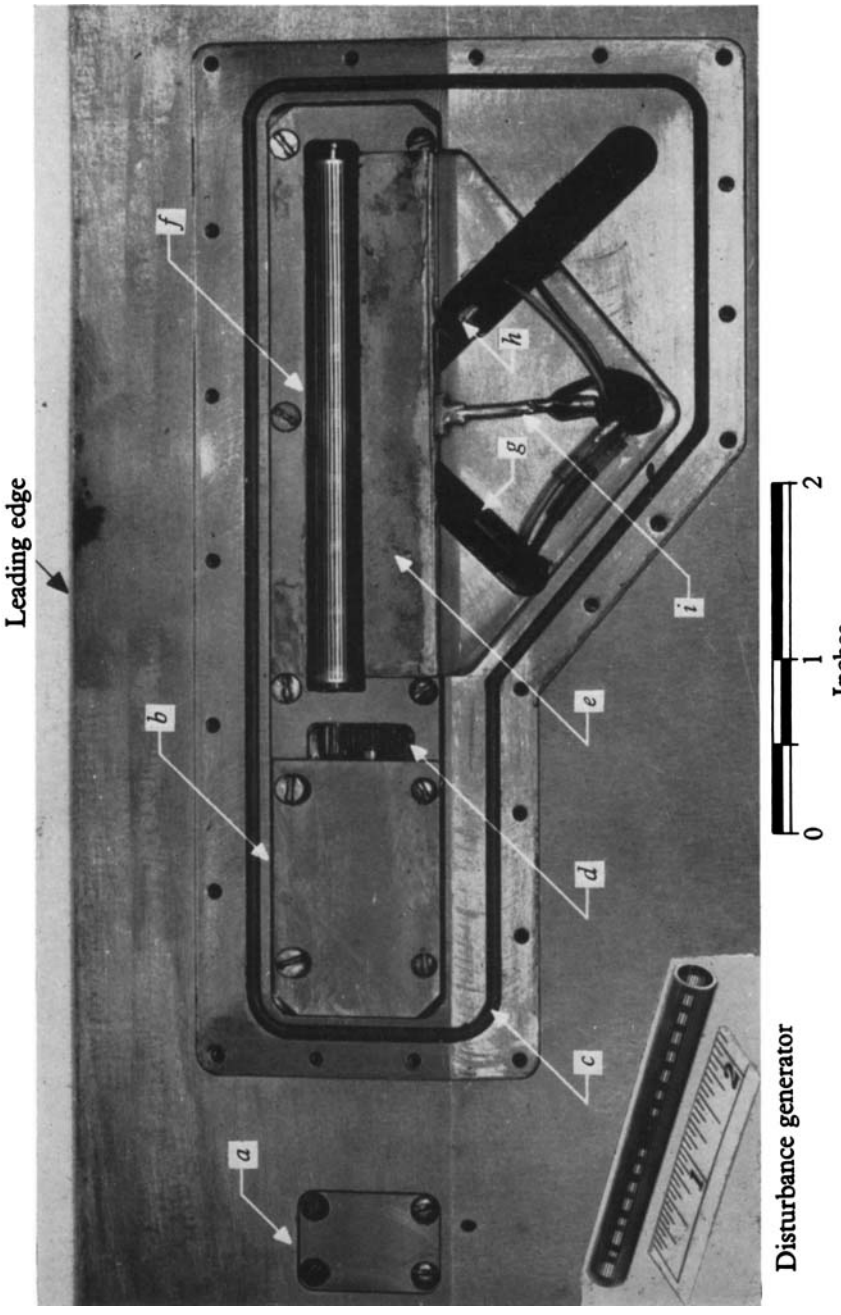

FIGURE 7. Disturbance generator installation in flat plate. *a*, bearing block; *b*, sealing block; *c*, O-ring; *d*, 2·5:1 gear; *e*, porous block; *f*, disturbance generator; *g*, light source; *h*, photo cell; *i*, air line.

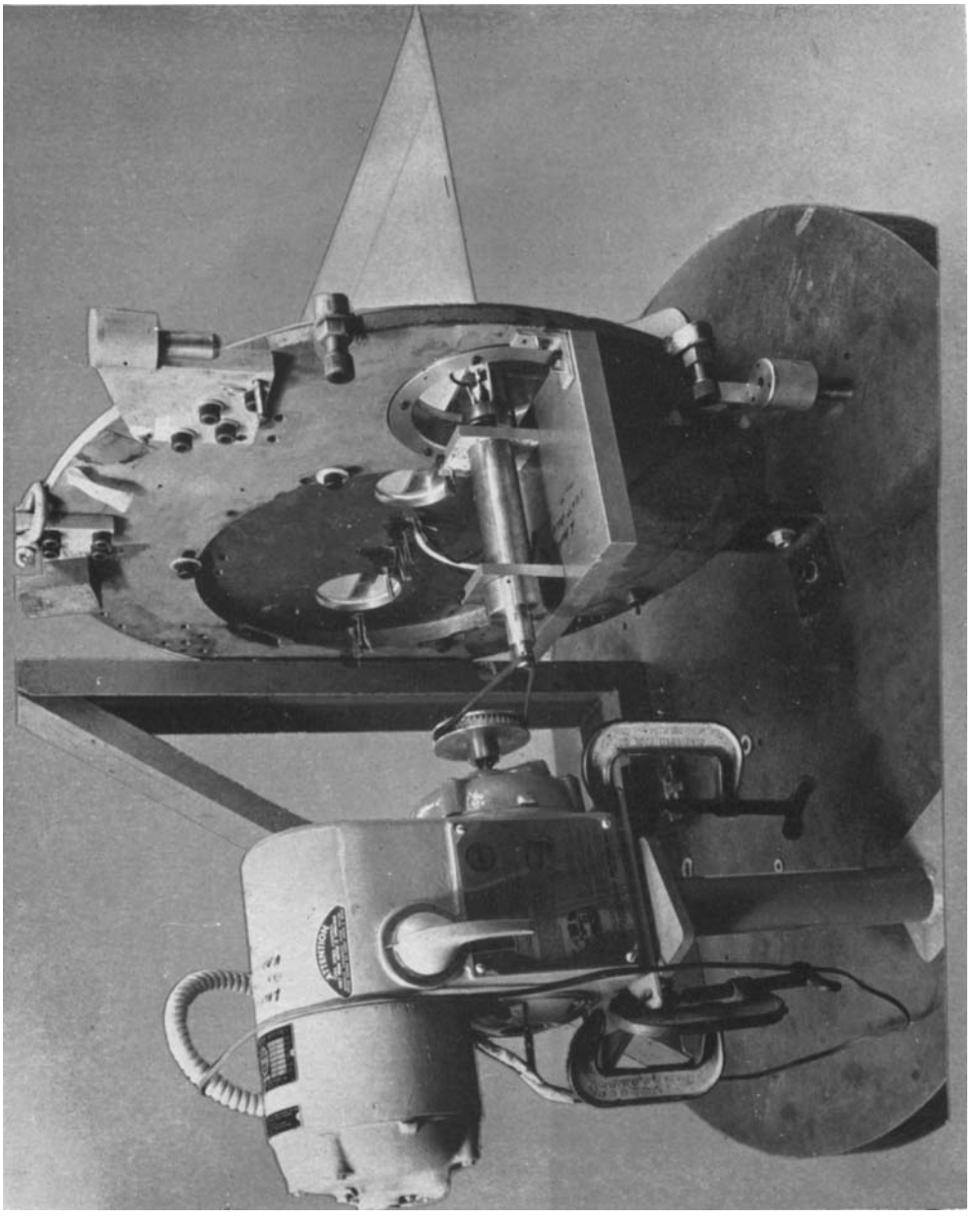

FIGURE 8. Varidrive motor and spindle installation for actuating disturbance generator.

vations, because of the great differences between the experimental environments, because of the magnitudes of the physical variables such as frequency and mean velocity in low speed and supersonic flow, and because of the more complicated flow field. Therefore, considerable time and effort were required before the existence of instability could be detected and the 'real' evidence isolated from

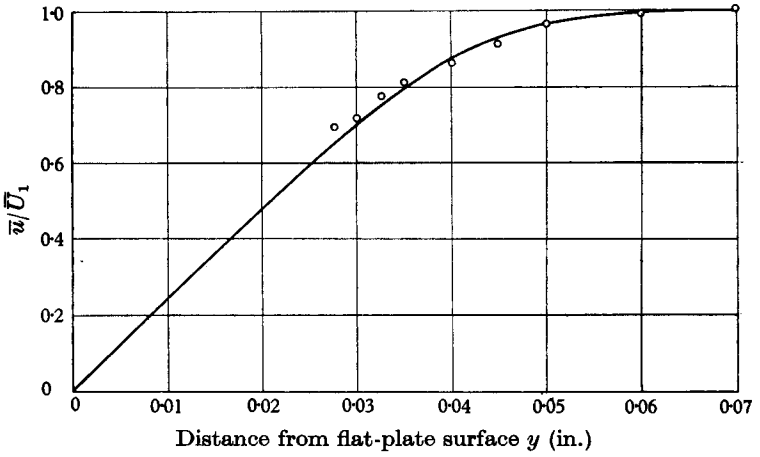

FIGURE 15. Mean velocity distribution across the boundary layer. $M_1 = 2{\cdot}2$, Re/in. = 77,000, $x = 5$ in.

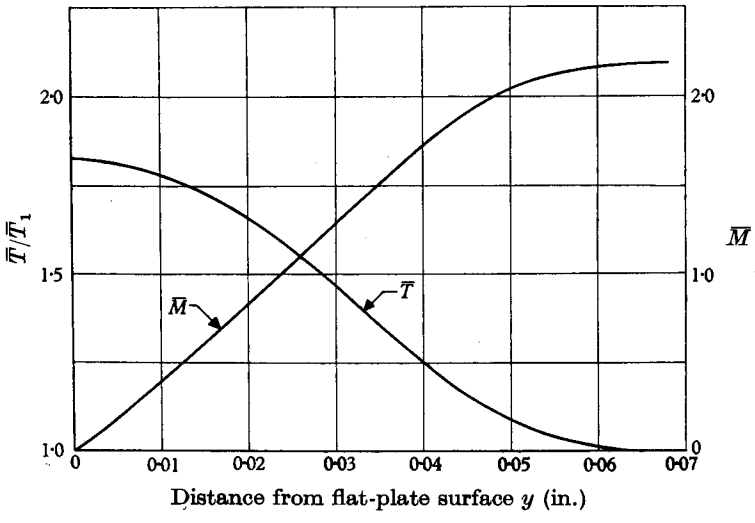

FIGURE 16. Mach number and temperature distribution across the boundary layer. $M_1 = 2{\cdot}2$, Re/in. = 77,000, $x = 5$ in.

the 'fictitious' evidence. A qualitative description of the observations identifying the instability will be given in § 5.2; a more critical and quantitative examination of the results will be made later.

The critical layer. It was noticed in the early phase of the experiments that even though the measurements of mean quantities had clearly demonstrated the laminar state of the boundary layer, the fluctuations within the layer were con-

siderably larger than those in the free stream. A detailed examination of their amplitude distribution across the layer indicated a remarkably sharp peak near the centre of the layer ($M_1 = 2{\cdot}2$), no matter at which x-station the measurement was carried out, including stations a few tenths of an inch ($R_\theta \approx 100$) from the leading edge. Figure 17 shows a typical distribution of the mean-square hot-wire output $\overline{e^2}$ across the layer, clearly exhibiting the peak. Incidentally, $\overline{e^2}$ corresponds approximately to the mean-square mass-flow fluctuations. It is well

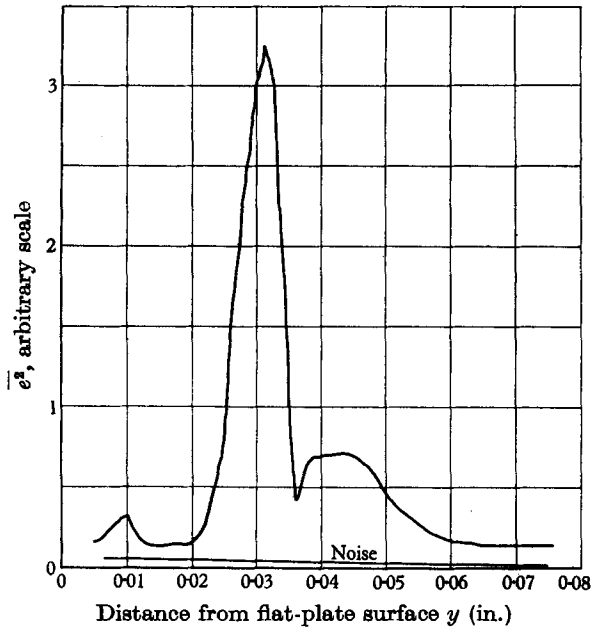

FIGURE 17. Distribution of the hot-wire output across the boundary layer. $M_1 = 2{\cdot}2$, Re/in. = 80,000, $x = 5{\cdot}0$ in.

known that such a peak is a characteristic feature of the self-excited instability oscillations in the incompressible laminar boundary layer (Schubauer & Skramstad 1948) and is the result of strong vorticity concentration at points where the local mean velocity is equal to the propagation velocity of the oscillations. Whereas in the incompressible case the peak was always located near the wall, in the present experiments for $M_1 = 2{\cdot}2$ the peak was found to be near the centre of the layer, indicating a higher ratio of wave velocity to free-stream velocity, as expected from theoretical calculations (Lees 1947).

Maximum amplification curves. Observation of the fluctuations on an oscilloscope did not reveal any periodic oscillations as reported by Schubauer & Skramstad. However, examination of the energy spectra indicated a characteristic maximum which shifted to lower frequencies as the distance from the leading edge x was increased, and at the same time the peaks were seen to be sharper. Figure 18 shows several such spectra. The question that immediately arises is whether the peaks are the result of the boundary-layer instability process. If indeed they are, it should be expected that the dimensionless frequencies

corresponding to the maxima be unique functions of the boundary-layer Reynolds number. This was examined by varying the Reynolds number two ways during the spectrum measurements: (1) spectrum data were taken at various distances from the leading edge while the tunnel pressure was kept constant; (2) the tunnel pressure was changed for each spectrum distribution obtained at a constant

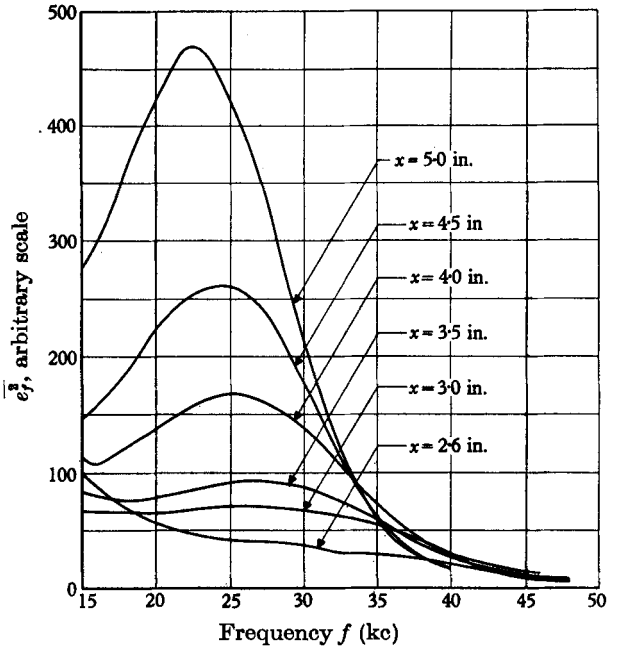

FIGURE 18. Energy spectra of the natural disturbances in the boundary layer at several x-positions. $M_1 = 2{\cdot}0$, Re/in. = 300,000.

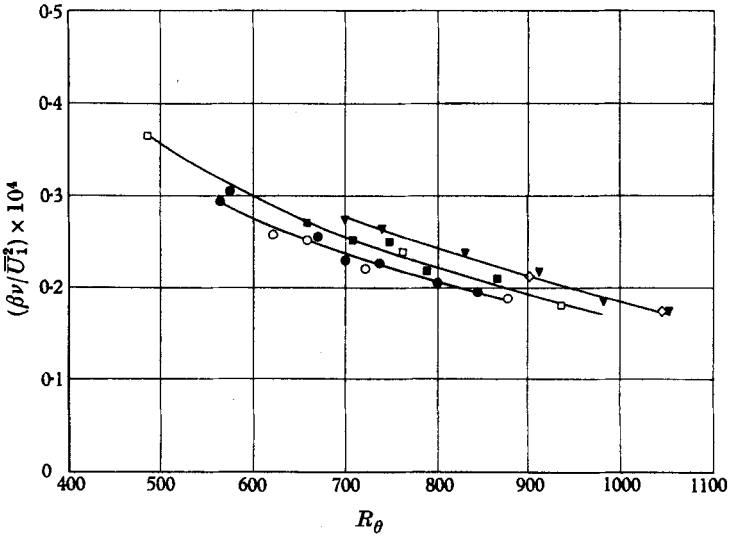

FIGURE 19. Maximum amplification curves. ◇, $M_1 = 1{\cdot}5$; ▽, $M_1 = 1{\cdot}6$; □, $M_1 = 2{\cdot}0$; ○, $M_1 = 2{\cdot}2$. Open symbols: stationary hot wire; solid symbols: moveable hot wire.

x-position. The results of the two sets of tests, indicated by open and solid symbols in figure 19, are seen to be consistent for each Mach number tested. It is further seen from figure 19 that the curves, usually referred to as the maximum-amplification curves, move to lower values of the non-dimensional frequencies as the Mach number increases. This tendency is expected from the stability calculations of Lees (1947). These measurements thus gave further clues that the observations must be related to the boundary-layer instability.

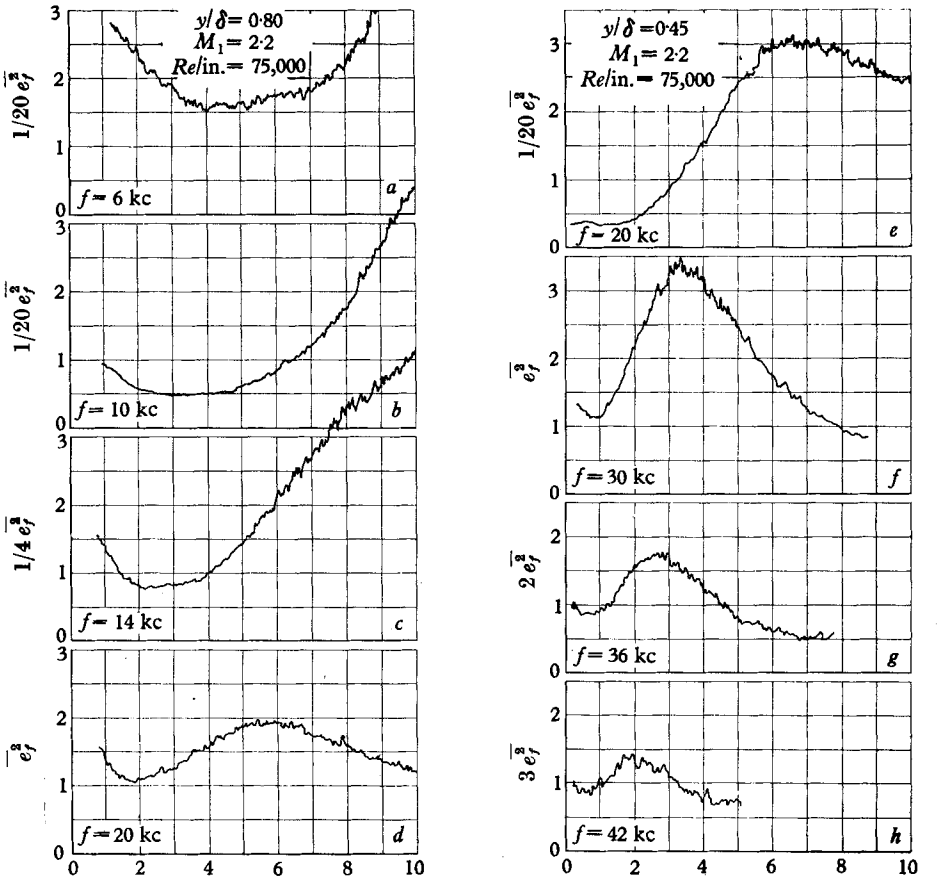

FIGURE 20. Variation of disturbance amplitudes along the flat plate at several frequencies.

Amplitude variations along the plate. The most direct and most positive evidence of the small-disturbance type of instability was obtained from the examination of the energy content of various narrow frequency bands at various distances from the leading edge. This kind of experiment was suggested by the well-known 'filtering action' of the boundary layer whereby it augments the energy in certain frequency bands of the disturbances and diminishes the energy in others, depending on the Reynolds number. Figure 20 shows such measurements carried out at Mach number 2·2 in the frequency range of 6 to 42 kc. These curves were

obtained by the method described in § 4.1; that is, the wire was moved along lines of constant y/δ and the signal was fed through a wave analyser. The ordinates of the various curves are comparable as indicated; the absolute scale, however, is arbitrary. It is seen in figure 20 that the curves exhibit a minimum or a maximum or both, demonstrating the amplifying and damping effect of the boundary layer. At the x-positions where the curves have negative slopes, the boundary layer is stable with respect to the disturbances and unstable where the slopes are positive.

5.3. *Disturbances present in the boundary layer*

The experiments that have been described gave strong evidence of the existence of self-excited oscillations in the boundary layer. However, before any quantitative conclusions are drawn from them, there are several points that should be further discussed.

Extraneous effects. Most of the experiments utilized the convenient (but not always desirable) free-stream disturbances as a means of studying the stability problem. The disturbances were found to be spatially homogeneous and to have a continuous energy spectrum, the energy decreasing with frequency. At the leading edge of the flat plate these disturbances are carried into the boundary layer and their energy spectra (corresponding to a constant y/δ) undergo certain changes along the plate. For the purpose of the present investigation, it is essential to know that these changes are due primarily to the stabilizing (or destabilizing) action of the boundary layer, and that secondary effects that also may influence the energy spectrum are negligibly small. Causes of such extraneous effects might be: (1) disturbances convected into the boundary layer along its outer edge by the mean mass influx; (2) interaction between disturbance energies corresponding to different frequency bands (this effect would rule out the use of disturbances having wide, continuous energy spectra); (3) strong interaction between the disturbances and the mean flow field.

In order to examine the importance of (1) and (2) above, an artificial disturbance of controlled frequency and amplitude was introduced near the leading edge, and its amplitude variation along the plate was studied. The initial amplitudes were chosen to be much larger than those of the natural disturbances but not large enough to disturb the mean flow field of the boundary layer. A comparison of the neutral curves (to be shown and discussed later) that were obtained using natural and artificial disturbances shows complete agreement. It may thus be concluded that any influence of these effects on the location of the stable and unstable regions is negligibly small.

The optimum amplitude for the artificial disturbances, incidentally, could be conveniently determined by observing the traces of the boundary-layer growth (see § 4.1). In figure 21 a typical example of the effect of excessive injection rate is given. The figure also shows the extreme sensitivity of the boundary-layer stability mechanism (and, incidentally, of the instrumentation) to any change in the mean flow field. The boundary-layer growth curves (designated by y), obtained with and without injection through the slot, do not coincide, indicating a change in the mean flow field. It should be remembered that through the servo

system the hot wire automatically seeks points of constant mean mass flow. Thus, as the boundary layer thickens because of an excessive injection rate, the hot wire moves a certain distance away from the wall. At the same time it is to be noted in figure 21 that the amplitude curves (designated by $\overline{e_f^2}$) do not peak at the same x-position. However, if the increase in boundary-layer thickness is taken into account, the neutral points correspond closely to the same value of the Reynolds number.

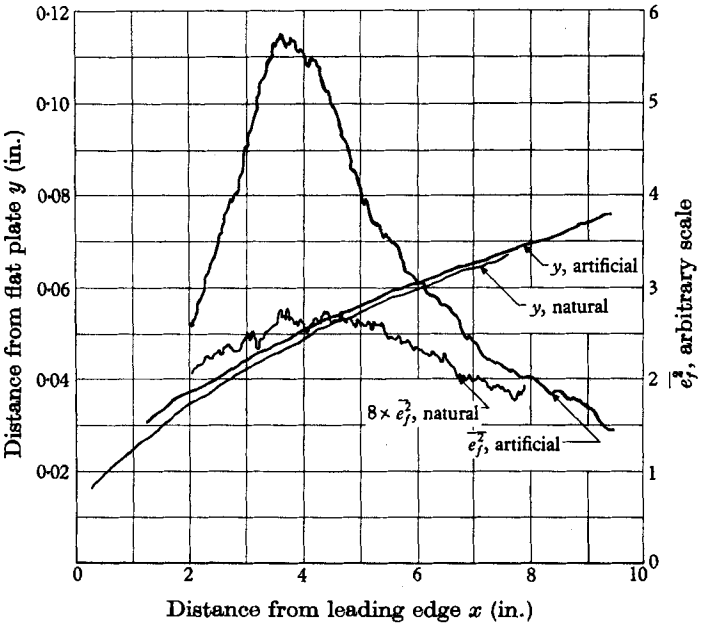

FIGURE 21. Variation of a natural and an artificial disturbance with corresponding boundary-layer growth curves. $M_1 = 2{\cdot}2$, Re/in. = 75,000, $f = 23$ kc.

Any further increase in the amplitude of the artificial disturbance resulted in a measurable change in the boundary-layer growth rate, indicating the presence of effect (3). If the non-linear interactions of the type listed under (3) are to be considered negligible, the amplitudes of the disturbances introduced in the boundary layer must be small in all the frequency bands. Of course, it is difficult to decide *a priori* what can be considered a small amplitude. One possibility would be by means of a comparison of stability results obtained using different initial disturbance amplitudes. Unfortunately, variation of the free-stream disturbance level for a given flow Mach number proved to be impractical. Instead, the stability measurements were repeated at various flow Mach numbers (1·6, 2·2, and 3·0) in which cases the free-stream mass-flow fluctuations were approximately 0·1, 0·2, and 0·4 %, respectively. It was established that the results at $M = 2{\cdot}2$ were consistent with those obtained at $M = 1{\cdot}6$; whereas at $M = 3{\cdot}0$ the detection of self-excited oscillations was much more difficult and less reliable. For this reason the experiments were limited to Mach numbers below 2·5.

Repeatability of the measurements. Once an acceptable upper limit to the free-stream disturbance amplitudes was decided on (that corresponding to $M = 2{\cdot}2$), it was not too difficult to ascertain that all subsequent measurements should be carried out within this amplitude limit. Since the position of transition from the laminar to the turbulent state is a sensitive indication of the disturbance amplitudes present in the boundary layer, an early transition immediately indicated excessive disturbances. The reason for this not too infrequent occurrence was traced to leaking nozzle seals or pressure holes or to damage on the flat-plate leading edge. However, once such a situation was remedied, all the measurements described here were well reproducible even if they were repeated after a considerable time interval (one year). The maximum shift in the neutral points seldom exceeded $\Delta R_\theta = 20$. The reliability of the measurements was further enhanced by the close agreement with the results obtained using artificial disturbances.

5.4. *Neutral stability curves and amplifications*

Examining the stability of the boundary layer with respect to a given disturbance, one is interested not in the absolute amplitudes of these perturbations but rather in their streamwise logarithmic derivatives (amplifications) along the plate. The boundary layer may then be considered stable at a given Reynolds number if

$$\frac{1}{\tilde{Q}}\frac{\partial \tilde{Q}}{\partial x} < 0,$$

and unstable if

$$\frac{1}{\tilde{Q}}\frac{\partial \tilde{Q}}{\partial x} > 0,$$

where $\tilde{Q}(x, y/\delta)$ is any quantity such as $\tilde{u}$, $\tilde{\rho}$, or $\tilde{T}$. The so-called neutral points where the logarithmic derivative vanishes correspond to the limits between the stable and unstable regions. Such a stability criterion, however, does not define a unique neutral curve as described below.

In figure 20 the hot-wire outputs $\overline{e_f^2}$ are plotted as a function of x. Since the logarithmic derivative of $\tilde{e}_f$ is equivalent to that of $\tilde{Q}$ (§ 4.1), the stability limits may therefore be determined from the curves of figure 20. According to the stability criterion given above, the extrema of the curves correspond to the neutral points; the x-location of a minimum indicates the beginning of the unstable region (lower-branch neutral point), and that of a maximum the end (upper-branch neutral point). In figure 22 the non-dimensional frequency is plotted against the positions of the corresponding neutral points expressed in terms of R_θ. The figure includes not only the neutral points from figure 20, but also those obtained at other tunnel Reynolds numbers and those obtained using artificial disturbances.

Figure 22 clearly shows that the stability limits so obtained depend on the value of y/δ at which the observations were made. The difference in the neutral curves is definitely within the accuracy limits of the measurements. Subsequent observations at higher tunnel pressures (to check for possible probe interference) and using artificial disturbances gave the same result.

In figures 20*d* and 20*e* one may directly compare two amplitude distributions ($f = 20$ kc) made at $y/\delta = 0{\cdot}8$ and $y/\delta = 0{\cdot}45$. The x-positions of the maxima and minima are noticeably different; furthermore, the minimum obtained at $y/\delta = 0{\cdot}8$ is much better defined that at $y/\delta = 0{\cdot}45$. As a matter of fact, for lower frequencies the minimum could be detected only with difficulty or not at all at $y/\delta = 0{\cdot}45$ (not shown).

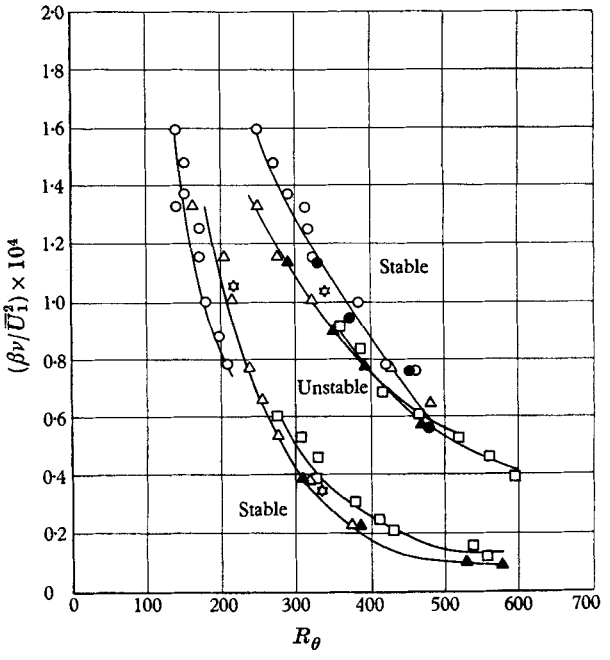

FIGURE 22. Neutral stability curve at $M_1 = 2{\cdot}2$.

	Disturbance	
y/δ	Natural	Artificial
0·34	□	
0·45	○	●
0·7–0·8	△	▲
Area method	✡	

The differences become even more apparent if the logarithmic derivatives for the two cases are compared. Figure 23 shows these derivatives in a non-dimensional form computed at various values of the Reynolds number. It is seen that the amplifications always appear smaller in the outer edge of the layer and that the difference becomes less apparent with increasing Reynolds number.

In order to further examine this problem, the stability criterion will now be expressed somewhat differently. We define a mean amplitude Γ averaged across the boundary layer (the use of a mean energy would lead to similar results),

$$\Gamma(x) = \int_0^1 \tilde{e}_f d\left(\frac{y}{\delta}\right);$$

and we propose to call the boundary layer stable where

$$\frac{1}{\Gamma}\frac{d\Gamma}{dx} < 0,$$

and unstable where

$$\frac{1}{\Gamma}\frac{d\Gamma}{dx} > 0.$$

This stability criterion is equivalent to the previous one if

$$\frac{1}{\Gamma}\frac{d\Gamma}{dx} = \frac{1}{\tilde{e}}\frac{d\tilde{e}}{dx} \quad \text{or} \quad \frac{\partial}{\partial x}\frac{\tilde{e}_f}{\Gamma} = 0$$

for all values of y/δ, that is, if the distribution $\tilde{e}_f/\Gamma$ is a function of y/δ only and thus follows the boundary-layer similarity. This condition will now be experimentally investigated. For the calculations of Γ, amplitude distributions across

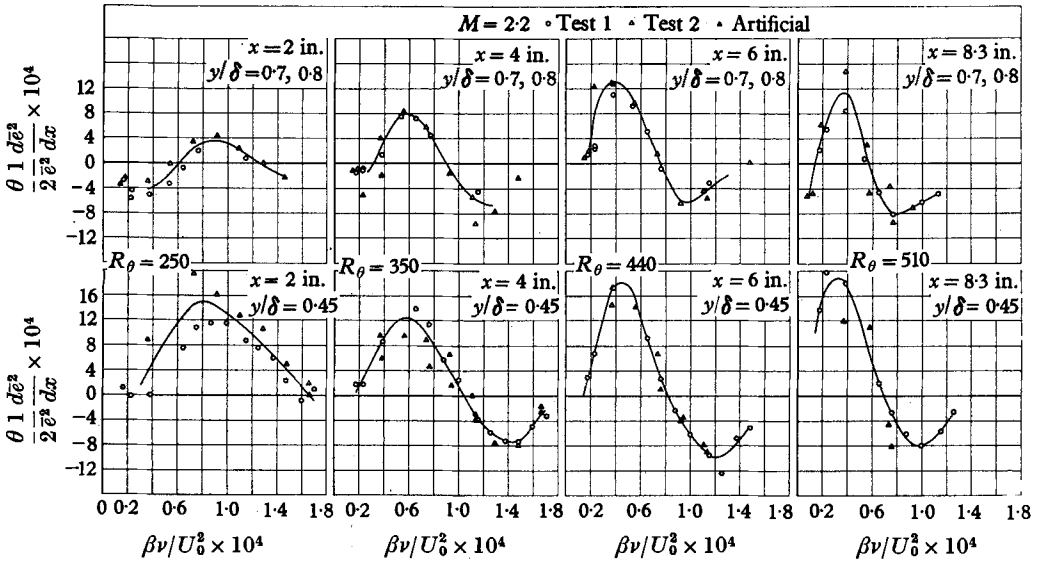

FIGURE 23. Amplification curves.

the layer were measured at various x-positions. A sample of such distributions corresponding to 30 kc frequency is shown in figure 24. (Incidentally, the typical maximum near the critical layer is already noticeable at $x = 0{\cdot}5$ in.; the curious secondary peaks will be discussed in § 5.5.)

In figure 25 the normalized amplitudes

$$\frac{\tilde{e}(x, y/\delta)}{\Gamma(x)}$$

are plotted against y/δ for various values of R_θ. (For clarity, not all the distributions are shown.)

Clearly, the above condition is not satisfied. Near the critical layer $(\partial/\partial x)\,(\tilde{e}_f/\Gamma)$ is positive, and near the free-stream end it is mainly negative. This explains why the

amplifications obtained at $y/\delta = 0{\cdot}45$ are larger than those at $y/\delta = 0{\cdot}8$ (figure 23), or why the unstable region corresponding to $y/\delta = 0{\cdot}45$ in figure 22 is wider.

Deciding which stability limits to adopt is really an academic question. In a comparison of disturbance amplitudes corresponding to the same mean flow

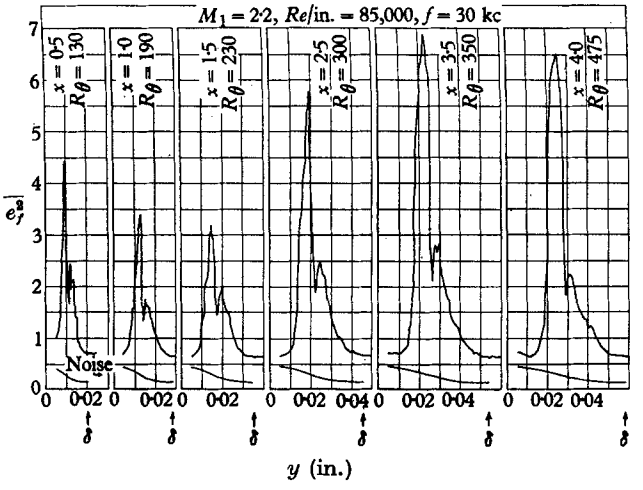

FIGURE 24. Amplitude distribution across the boundary layer of a fixed-frequency disturbance at several x-positions.

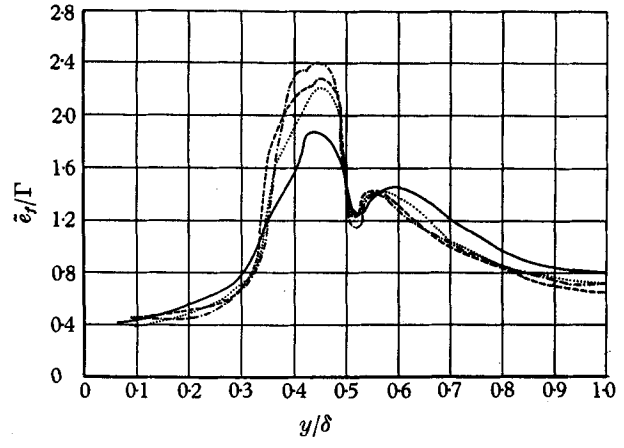

FIGURE 25. Normalized amplitude distributions. $M_1 = 2{\cdot}2$, Re/in. = 85,000, f = 30 kc.

	x (in.)	R_θ
———	1·5	230
.....	2·5	300
– – – – –	3·5	350
—·—·—	4·5	400

conditions (constant y/δ), the physical fact is that disturbances are amplified more near the critical layer than near the inner and outer edges of the boundary layer, especially for low Reynolds numbers. Should one want to talk about a unique neutral curve, the second stability criterion is preferable. Using this criterion, some calculated neutral points are shown as stars in figure 22.

5.5. *Amplitude distributions across the boundary layer*

In the previous section some distributions in terms of the hot-wire output $\overline{e_f^2}$ have been shown (figure 24). The behaviour of the velocity, temperature, and pressure fluctuations across the layer will now be examined.

An artificial disturbance having a frequency of 23 kc ($\beta\nu/U_1^2 = 0{\cdot}85 \times 10^{-4}$) was chosen for the experiment and was examined at a position $x = 5$ in. ($R_\theta = 400$). This approximately corresponded to a point on the upper branch of the neutral stability curve. In order to express the hot-wire output voltages in

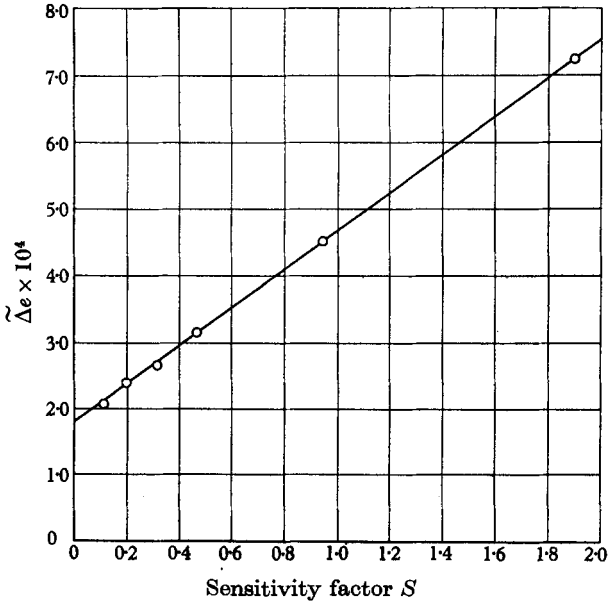

FIGURE 26. Fluctuation mode diagram in the free stream near the edge of the boundary layer. $M_1 = 2{\cdot}2$, Re/in. = 77,000.

terms of the flow quantities, the method suggested by Kovasznay (1953) was applied. As is well known, only two of the perturbations, mass-flow

$$[m'/\overline{m} = \rho'/\overline{\rho} + u'/\overline{u}]$$

and total temperature $\quad [T_T'/\overline{T}_T = \alpha(T'/\overline{T}) + \beta(u'/\overline{u})]$

fluctuations can be obtained (see equation (5.1)) in the range $M > 1{\cdot}2$. Typical raw data of the hot-wire output are shown in figure 17. The measurements resulted in mode diagrams similar to that shown in figure 26, indicating that inside the layer, just as outside, $\tilde{m}/\overline{m}$ and $\tilde{T}_T/\overline{T}_T$ appear to be perfectly anti-correlated (the points in the diagram define a straightline). From such diagrams the mass-flow and total-temperature fluctuations may be directly computed; the result is plotted in figure 27. The very pronounced peak near the critical layer ($y \approx 0{\cdot}28$ in.) is well illustrated.

Unfortunately, a result of this nature is not very instructive unless the three basic fluctuation quantities can be separated. In order to do this it is necessary

to make an assumption concerning the fluctuation field. Outside the boundary layer, in the potential field of the oscillation, this does not present a problem. Here isentropic relations between the temperature and density fluctuations exist and they can therefore be calculated separately (see § 5.6). Inside the boundary layer, however, the situation is different: the dominating action of viscosity near the wall and at the critical layer prevents the making of such an

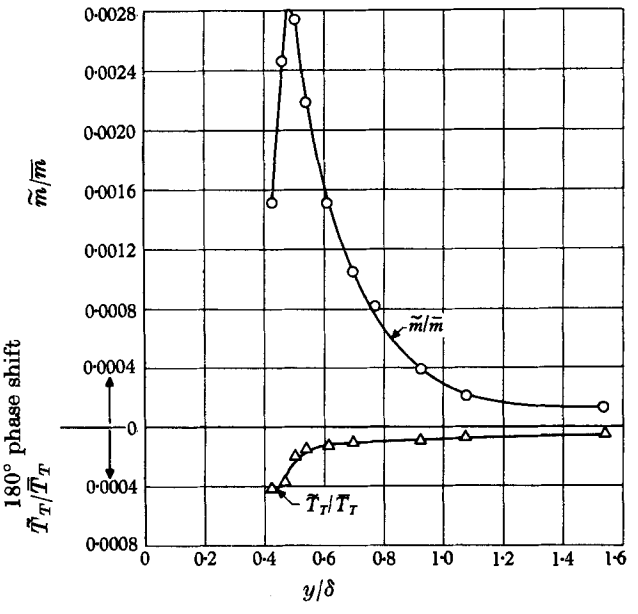

FIGURE 27. Mass-flow and total-temperature fluctuations in the boundary layer. $M_1 = 2{\cdot}2$, $Re/\text{in.} = 77{,}000$, $x = 5$ in.

assumption. Another simplification is used instead, based on the following qualitative argument. A wave motion superimposed on the boundary layer produces a pressure gradient $\partial\tilde{p}/\partial y$ that diminishes with decreasing wave amplitude and increasing wavelength. Since $v'/\bar{u}$ is small and the wavelength is large (approximately 10δ) in the present experiments, it will be assumed that $\partial\tilde{p}/\partial y$ is small and thus $\tilde{p}$ is constant across the layer. The magnitude of $\tilde{p}$ was calculated from the mass-flow fluctuation measurement near the edge of the boundary layer ($y/\delta = 1{\cdot}08$), using isentropic relations between the perturbations. Since the phase relation between the pressure and the velocity (or temperature) fluctuations is not known (except the fact that they are in phase or 180 degrees out of phase), two distributions of these quantities are obtained from the hot-wire equations. One set of roots, for instance, results near the critical layer in a positive pressure-temperature correlation if one chooses negative pressure-velocity correlation, and vice versa.

Without additional information it is not possible to choose which of the two sets of roots is the correct one. It was necessary to refer to the solution of the perturbation equations (3.1–3.11) to decide on this. For this purpose the inviscid equations of motion were integrated in the outer half of the boundary

layer using the theoretical eigenvalues,* and the results were compared with the corresponding distributions calculated from the measurements. The amplitude of the computed mass-flow fluctuations was matched to the measured value at $y = \delta$, and the theoretical results were plotted as thin solid lines in figure 28. It is seen that the theoretical pressure fluctuations indeed are fairly constant within about 15 %, at least in the outer half of the boundary layer.† Thus, the assumption of constant $\tilde{p}$ used in the reduction of the measured data is justified. The symbols in figure 28 correspond to the roots of the hot-wire equations nearest the

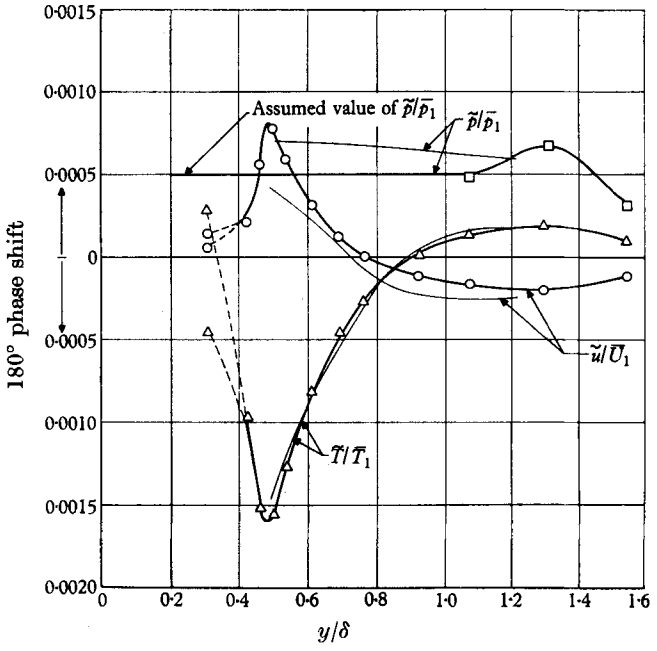

FIGURE 28. Velocity, temperature, and pressure fluctuations in the boundary layer.
$M_1 = 2{\cdot}2$, $Re/\text{in.} = 77{,}000$, $R_\theta = 400$, $c/\bar{U}_1 = 0{\cdot}62$.
Experiment: ○, $\tilde{u}/\bar{U}_1$; △, $\tilde{T}/\bar{T}_1$; □, $\tilde{p}/\bar{p}_1$.
Theory ($R_\theta = 440$, $c/\bar{U}_1 = 0{\cdot}616$): ———.

theoretical curves. Since the second set of roots defines a completely different velocity and temperature distribution, it was not difficult to pick out the correct roots. The only exception was the point nearest the wall ($y/\delta = 0{\cdot}31$); in this case both roots are shown. Incidentally, this point corresponds to a position where $M = 0{\cdot}8$, and the more general hot-wire equations suggested by Morkovin (1956) were used in reducing the data. It should also be mentioned that since the hot-wire sensitivities at transonic flows are not well established, the measurements here are less reliable.

The root-mean-square values of the various fluctuations in figures 27 and 28 were plotted in a fashion that shows the phase relations between them. It was mentioned earlier that these fluctuations were always either in phase or 180

* The authors are grateful to Dr L. Mack for providing these calculations.

† Some recent calculations of Dr E. Reshotko show that this is true across the whole layer.

degrees out of phase with each other. In the figures the phase relations with respect to the pressure fluctuations are indicated: in-phase fluctuations are plotted in the positive sense, out-of-phase ones in the negative sense. For instance, outside of the boundary layer where the isentropic relations hold between pressure, density, and temperature fluctuation (they are all in phase), the temperature fluctuations are plotted in the positive sense. It is interesting to notice that inside the layer not only the velocity oscillations (as found in the incompressible case), but also the temperature oscillations undergo a 180-degree phase shift.

At this point a comment is in order on the secondary peaks clearly shown in the distributions figure 24. These peaks were almost always present (also with artificial disturbances) when measurements were made at high mean-wire temperatures; at low temperatures, only a small peak or no peak was observed. Thus, the secondary peaks are believed to be the result of a curious combination of the hot-wire response and the particular distribution of the velocity, temperature, and density fluctuations.

One of the most striking features of the fluctuation distributions shown in figure 28 is the large amplitude of the temperature (and density) distribution near the critical layer. Since the mean temperature gradient in the boundary layer increases rapidly with Mach number, such a result is not surprising. As a matter of fact, with increasing free-stream Mach number the temperature and density fluctuations will become more and more important. From the continuity and energy equations (3.7) and (3.10), one obtains, neglecting conductivity,

$$\left(1-\frac{c}{\bar{u}}\right)\left[\frac{\theta}{\bar{T}}-(\gamma-1)\frac{r}{\bar{\rho}}\right]=\frac{i\gamma}{\alpha\bar{T}}\frac{d\bar{T}}{dy}\frac{v'}{\bar{u}}.$$

In the region of our interest, near but just outside the critical layer where the non-viscous approximation is still valid, the temperature and density fluctuations are 180 degrees out of phase. Therefore, in terms of root-mean-square values, the above equation becomes

$$\frac{\frac{\tilde{\theta}}{\bar{T}}+(\gamma-1)\frac{\tilde{r}}{\bar{\rho}}}{\frac{1}{\alpha\delta}\frac{\tilde{v}}{\bar{u}}}=-\frac{1}{1-\frac{c}{\bar{u}}}\frac{\gamma}{\bar{T}}\frac{d\bar{T}}{d\frac{y}{\delta}}.$$

The right side of the equation increases rapidly with Mach number; thus, for a given disturbance, $(\tilde{v}/\bar{u})\,(1/\alpha\delta)$ constant, the temperature and density fluctuations become large indeed.

5.6. *The propagation velocity*

From theoretical considerations it is expected that once a disturbance is introduced locally into the boundary layer it will develop into a wave motion having a definite wave velocity and amplitude variation. The latter has already been discussed; it remains to be shown experimentally that the motion is wave-like. This was done by two different methods: (1) by measurement of the wavelength and (2) by a more indirect technique.

(1) The determination of the wavelength of an artificial disturbance of known frequency was described in § 4.2, and a typical result is shown in figure 29. The plot, which incidentally is raw data, indicates unquestionably the wave character of the disturbance and provides the wavelength directly. From the measured wavelength corresponding to the neutral point and from the known frequency, the velocity of a neutral wave can be obtained.

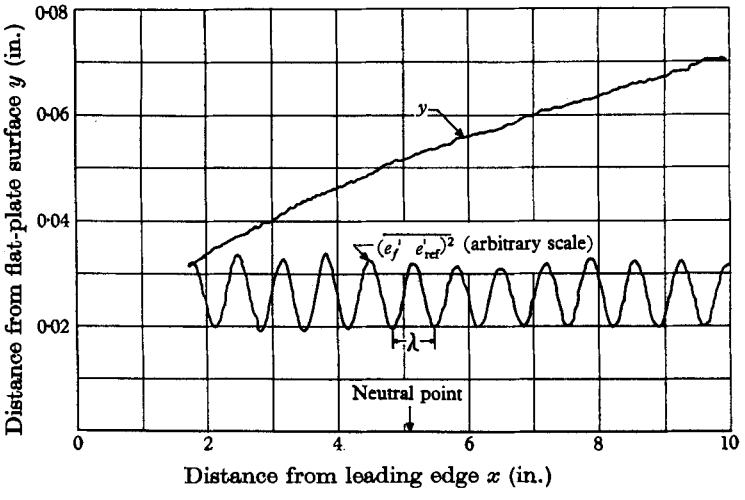

FIGURE 29. Wavelength measurements of an artificial disturbance. $M_1 = 2{\cdot}2$, $Re/\text{in.} = 77{,}000$, $f = 19{\cdot}6$ kc.

(2) The alternative method is based on the idea that if the artificial disturbance indeed develops into a wave motion, the boundary layer may be considered a moving wavy wall. From the measurements of the pressure and velocity fluctuations in the potential field just outside the layer, the velocity of the wavy wall can be calculated. Clearly, from such an indirect method it is not expected to obtain accurate values of c (especially since c is only approximately constant along x). Nevertheless, the method is described here in order to show that with the present hot-wire technique measurements of fluctuations in supersonic flows may be made with confidence.

The general hot-wire equation

$$\Delta e = \alpha \frac{T'}{\overline{T}} + \beta \frac{u'}{\overline{u}} - S\left(\frac{\rho'}{\overline{\rho}} + \frac{u'}{\overline{u}}\right) \tag{5.1}$$

may be put in a simpler form, since outside the boundary layer an isentropic relation between the fluctuations may be assumed:

$$\Delta e = \alpha(\gamma - 1)\left[\frac{\rho'}{\overline{\rho}_1} + M_1^2 \frac{u'}{\overline{U}_1}\right] - S\left[\frac{\rho'}{\overline{\rho}_1} + \frac{u'}{\overline{U}_1}\right],$$

where

$$\alpha = \left(1 + \frac{\gamma - 1}{2} M_1^2\right)^{-1}$$

and

$$\beta = (\gamma - 1)\alpha M_1^2.$$

Figure 26 shows that $\Delta\tilde{e}$ is a linear function of S, indicating that the total-temperature (first term) and mass-flow (second bracketed term) fluctuations are perfectly anticorrelated, consistent with the assumption of isentropy. From mode diagrams such as figure 26, the velocity and density fluctuations (also $\tilde{p}$ and $\tilde{T}$) may be obtained. From the potential solution of a moving wavy wall (Liepmann & Roshko 1957) and from the measured $\tilde{u}$ and $\tilde{\rho}$, the velocity of the wall may be calculated:

$$\frac{c}{\overline{U}_1} = 1 - \frac{\tilde{p}/\overline{p}_1}{\gamma M_1^2 \tilde{u}/\overline{U}_1}.$$

For the conditions represented in figure 26 the wave velocity was found to be $c/\overline{U}_1 = 0{\cdot}60$, which compares well with the value of 0·62 obtained from phase measurement.

5.7. *Comparison with theory*

The results that have been described confirm qualitatively the predictions of the stability theory: the existence of unstable oscillations in a supersonic boundary layer; the wave-like character of the oscillations; and the existence of an inner layer within the boundary layer where the amplitude of the oscillations is much larger than outside it. In this section a more quantitative comparison will be made in the light of the various assumptions of the theory.

Amplitude of the perturbations. In order to be able to compare the experimental results with the linear theory, it is necessary, of course, to ascertain that the disturbances studied in the experiments are small (assumption 1 of § 3.1). In the incompressible case it was shown recently by Schubauer (1958) that provided the velocity disturbances do not exceed an amplitude of 1–2 % of the free-stream velocity, the use of a linear theory for predicting their behaviour is justified. On the basis of the results described subsequently (§ 5.8), the same criterion may be used for the compressible case.

In the present experiments using artificial disturbances, it is estimated, based on the results of figure 28, that the fluctuation levels did not exceed the 0·5 % value. (The amplitudes of the natural disturbances were, of course, even smaller.) On this basis, therefore, a comparison of the experimental results with a linear theory is justified.

Two- and three-dimensional disturbances. The question arises whether a two- or three-dimensional theory should be used in the comparison. In the incompressible boundary layer this problem was not essential since, as pointed out recently by Lin (1958), the neutral curves for the two cases are almost identical.

In the present experiments the natural disturbances were certainly three-dimensional, while the artificial ones—although not purely two-dimensional—could be considered as containing predominantly two-dimensional disturbances. Nevertheless, the measurements made by both types of perturbations produced the same results concerning the stability limits and amplifications. On the basis of this evidence it may be assumed, therefore, that at least up to $M = 2{\cdot}2$ the stability of the boundary layer with respect to a two- and a three-dimensional disturbance does not change measurably. This is in agreement with the conclusion reached by Dunn & Lin (1955). Because of the approximations involved,

their result cannot be extended beyond a Mach number of approximately 1·8; but within this range they show that the three-dimensional disturbances are less important than the two-dimensional ones and become dominant only for the case of a cooled boundary layer.

On the basis of the above discussion the results of the two-dimensional theory will be used for the comparison with the experimental findings.

Neutral curves. Before making a quantitative comparison between the theoretical and experimental results, a fundamental difficulty has to be pointed out.

Let us first examine the problem considered by the theory: it is a non-stationary one in which the boundary layer of constant thickness (fixed R_θ) is perturbed at time $t = t_0$. The amplitude of the disturbances, Q', is then examined to determine how it changes for $t > t_0$. If the damping coefficient

$$\frac{1}{Q'}\frac{dQ'}{dt} \equiv \beta_i$$

is positive, the boundary layer is said to be unstable at R_θ with respect to the disturbance considered.

On the other hand, the experimenter faces a quasi-stationary problem: a disturbance introduced at the leading edge propagates along the layer, its amplitude changing in space and time. Thus, at a fixed R_θ one cannot measure a damping coefficient in the sense of the theory since the disturbance, the amplitude of which is observed at $t = t_0$, propagates into a region of increasing R_θ at $t > t_0$. What one can do is to measure at one fixed point in the layer the temporal mean value of Q' and observe how this value changes with x; thus, one can calculate an amplification defined as $(1/\tilde{Q})\,(d\tilde{Q}/dx)$. The basic difficulty now is to interpret this quantity in terms of the damping coefficient β_i of the theory. The general mathematical problem is a difficult one and no attempt is made here to discuss it; only one particular aspect will be considered.

It would be desirable to set up a simple criterion indicating the conditions under which comparison between the quantities β_i and $(1/\tilde{Q})\,(d\tilde{Q}/dx)$ could be made directly. In the past the two quantities were compared directly as follows: the disturbance being propagated by its eigenvelocity, $c = dx/dt$, served as the required transformation between the space and time co-ordinates; consequently it was postulated that

$$\frac{1}{\tilde{Q}}\frac{d\tilde{Q}}{dx} = \frac{1}{Q'}\frac{dQ'}{dt}\frac{dt}{dx} = \frac{\beta_i}{c}.$$

This procedure, however, is not strictly correct. It should be remembered that the amplitude function q as shown in equation (3.1) implicitly depends on the eigenvalues of the problem, thus in particular on the Reynolds number. Therefore, as the variation of Q with x is measured, keeping y/δ constant, R_θ changes (the boundary layer thickens) and, as mentioned above, q changes also. Therefore, the above equation must contain a term that takes into account this change. Thus, one may formally write

$$\frac{1}{\tilde{Q}}\frac{d\tilde{Q}}{dx} = \frac{1}{q}\left(\frac{\partial q}{\partial x}\right)_{y/\delta} + \frac{\beta_i}{c}.$$

In principle, both quantities on the right-hand side could be calculated from the theory and then their sum compared with the measured amplification $(1/\tilde{Q})\,(d\tilde{Q}/dx)$. This, however, has not been done, mainly because of the extremely time-consuming calculations involved. Instead, one may set up the criterion that the experimental amplifications can be compared directly with the theoretical damping coefficients only if the condition

$$\frac{1}{q}\left(\frac{\partial q}{\partial x}\right)_{y/\delta} \ll \frac{1}{\tilde{Q}}\frac{d\tilde{Q}}{dx}$$

is satisfied.

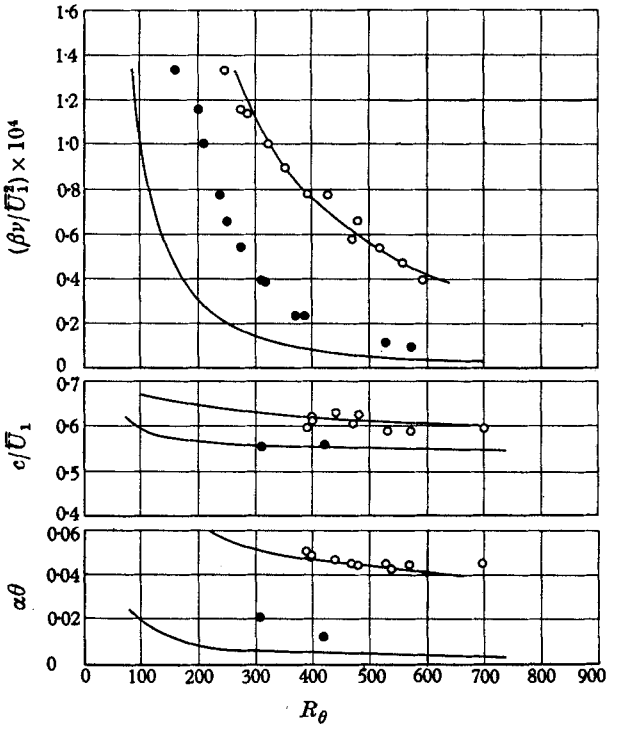

FIGURE 30. Theoretical and experimental neutral stability curves at $M_1 = 2{\cdot}2$. Experiment: ○, upper branch; ●, lower branch. Theory: ——.

This inequality can easily be checked from the plots shown in figure 25. The above condition implies that the amplification distributions with frequency be the same for all values of y/δ for a given Reynolds number. It is seen that on the outer edge of the boundary layer and for R_θ larger than approximately 300, this is approximately satisfied.

With the above limitation in mind we may proceed now to discuss the experimental results in the light of the theory. Accordingly, only the amplification measurements far from the critical layer are considered ($y/\delta \approx 0{\cdot}8$). In figures 30 and 31 the theoretical curves were calculated by Mack (1960), using the method proposed by Dunn & Lin (1955).

Considering first the velocity neutral curves of figures 30 and 31, one may easily verify that in all cases the propagation velocities of the self-excited oscilla-

tions are always subsonic with respect to the free stream. As discussed in § 3.1, this was an important assumption (assumption 4) of the theory that hereby finds complete verification. It is also seen that the absolute values of the velocities are in very good agreement with the theoretical predictions, with the possible exception of the lower branch points at $M = 1{\cdot}6$. (The measurements of the larger wavelengths, corresponding to the lower branches, were found to be more difficult.)

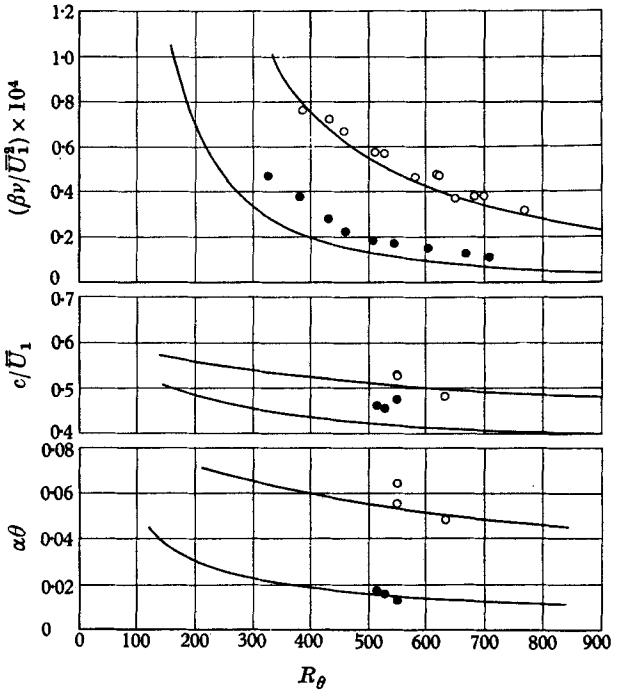

FIGURE 31. Theoretical and experimental neutral stability curves at $M_1 = 1{\cdot}6$. Experiment: ○, upper branch; ●, lower branch. Theory: ——.

Regarding the frequency neutral curves in these figures, the upper branches of the experimental and theoretical neutral curves agree satisfactorily. On the other hand, there is considerable discrepancy, especially at $M = 2{\cdot}2$, between the lower branches. Since the lower branches depend mainly on the viscous solutions of the stability problem, the source of the difficulty is believed to lie in these solutions.*

5.8. *Effect of compressibility on boundary-layer stability*

With the present formulation of the mathematical stability problem, it is not possible to answer easily the question of whether compressibility increases or decreases the stability of an adiabatic laminar boundary layer. As a matter of fact, one may arrive at a wrong conclusion by considering only certain phases

* In a recent work, Dr E. Reshotko critically examines the stability problem at supersonic Mach numbers and discusses this problem further.

of the problem. For instance, the supersonic inviscid boundary layer can be shown to be unstable, while the incompressible one is stable; also, from the expression of the minimum critical Reynolds number derived by Lees (1947), it is found that it decreases with increasing Mach number. From both of these results an erroneous conclusion could be drawn. Only the elaborate numerical calculations of Lees concerning the maximum amplification ratios of a disturbance give an indication of greater stability as the free-stream Mach number increases (Lees 1952). Under these circumstances it is most desirable if on the basis of the experimental findings some correlation could be found between the incompressible and compressible stability data from which the question posed above could be more readily answered. This problem will now be examined.

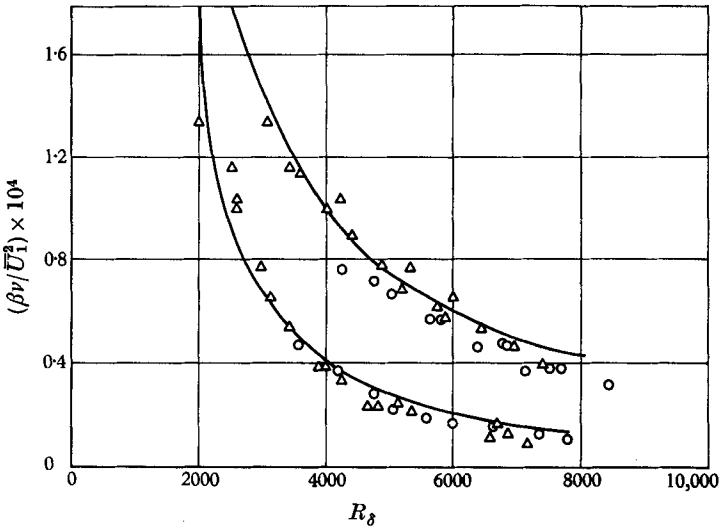

FIGURE 32. Experimental neutral stability curves.
——, $M = 0$ (Schubauer–Skramstad); ○, $M = 1{\cdot}6$; △, $M = 2{\cdot}2$.

The results of the theoretical eigenvalue calculations are usually presented in terms of the boundary-layer momentum thickness as the characteristic length. This is done mainly because, for a given x, the momentum thickness θ is practically constant over a wide range of Mach numbers. Considering now the frequency neutral curves as a function of R_θ for various Mach numbers (figures 30 and 31), it was noticed that the curves were similar but displaced in R_θ. Next to be examined was the question of whether by stretching the characteristic length the neutral curves could be correlated. The fact that the well-known Howarth co-ordinate transforms (with some additional minor assumptions) the compressible velocity distribution into the incompressible one suggests the use of the velocity instead of the momentum thickness as the characteristic length. In figure 32 the frequency neutral curves obtained at $M = 0$ by Schubauer & Skramstad (1948) are compared with those measured at $M = 1{\cdot}6$ and $2{\cdot}2$ on the basis of the velocity thickness Reynolds number. The agreement is surprisingly good.

Indeed a correlation exists, not only for the neutral oscillation, but for the amplified oscillations also. Considering sufficiently high Reynolds numbers for reasons already discussed in § 5.7, we may write

$$\frac{1}{2\bar{e}^2}\frac{d\bar{e}^2}{dx} = \frac{1}{\bar{Q}}\frac{d\bar{Q}}{dx} = \frac{\beta_i}{c},$$

or, in non-dimensional form,

$$\frac{\delta}{2\bar{e}^2}\frac{d\bar{e}^2}{dx}\frac{c}{\overline{U}_1} = \frac{\beta_i\delta}{\overline{U}_1}.$$

The calculation of the amplification coefficient involves a differentiation of the amplitude measurements, resulting in some scatter. Nevertheless, within the accuracy of the results a satisfactory agreement between the incompressible

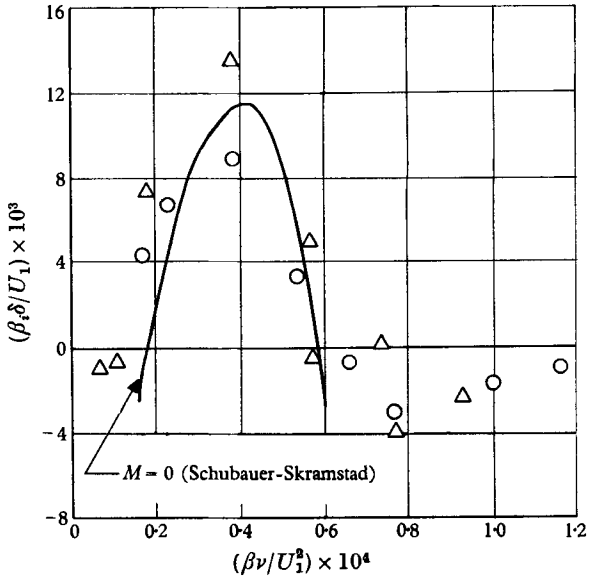

FIGURE 33. Amplification coefficients.
○, test 1; △, test 2; $M = 2{\cdot}2$; $y/\delta = 0{\cdot}7$, $0{\cdot}8$; $R_\delta = 6400$.

amplification coefficients and those at $M = 2{\cdot}2$ for approximately the same R_δ (figure 33) is obtained. For the propagation velocity the value $c = 0{\cdot}58$ was used, although it actually changed from $0{\cdot}55$ to $0{\cdot}61$ in the frequency range considered.

On the basis of the comparisons made, it is seen that in the Mach and Reynolds number ranges under consideration the stability limits of a disturbance of given frequency depend only on the local thickness δ and are independent of the Mach number. Furthermore, it is apparent that the non-dimensional amplification coefficient that is the temporal amplification rate $\beta_i\delta/\overline{U}_1$ corresponding to a given R_δ and frequency also is unaffected by the Mach number. On the other hand, the spatial amplification rate

$$\frac{\delta}{\bar{Q}}\frac{d\bar{Q}}{dx} = \frac{\beta_i\delta}{c}$$

decreases with increasing Mach number.

These conclusions are a consequence of the empirical results previously described. Unfortunately, the authors have been unsuccessful so far in finding a satisfactory explanation for this surprisingly simple correlation within the framework of the present theory. Only some rather general inferences may be drawn as follows. In the Mach number range considered, the boundary-layer stability is affected mainly by the change in the mean flow field (by the existence of mean density and temperature gradients), while the density and temperature fluctuations do not play an important role. (Roughly speaking, this implies the result of Lees & Lin (1946), who showed that the relation between the eigenvalues is independent of the temperature fluctuations.) Furthermore, as a result of this change in the mean flow field the disturbance of a given frequency acquires a larger wavelength; that is, the disturbance propagates faster downstream. As a consequence, the oscillations that have the same amplification coefficients have less time available to grow in amplitude over a given length of surface. Thus, a compressible boundary layer is more stable than the incompressible one.

5.9. *Effect of Mach number on transition*

Despite the great practical importance of the transition problem, as yet no reliable information, either experimental or theoretical, is available for the case of an adiabatic surface with zero pressure gradient. Specifically, it is not possible to make a definitive statement on the variation of transition Reynolds number with Mach number. Under the circumstances, therefore, it is worthwhile to examine the possibility of estimating, even in a crude fashion, the effect of compressibility on transition Reynolds number, using the present results.

As mentioned already in § 1, the Tollmien–Schlichting instability mechanism is only the initial stage of the transition process; therefore, at least in principle, it is not justifiable to use the linear theory for predicting the point of transition. However, in the incompressible case some favourable circumstances are known to exist which, at least for engineering purposes, permit the use of the linear theory. Some recent work of Schubauer (1958) and Klebanoff & Tidstrom (1959) indicates that the distance interval between the point of transition, x_t, and the point where the linear approximation becomes invalid, x_e, is small compared with x_t, and that the breakdown into turbulent spots occurs at approximately the same oscillation amplitude ($\tilde{u}/\overline{U}_1 \approx 7\,\%$). The fair success of the method proposed by Smith (1956) in predicting transition Reynolds numbers, using a linear theory, is believed to hinge on these experimental findings.

Unfortunately, in the compressible case very little is known at present about the non-linear region of transition. From the lower amplification rates obtained in the present work, it is expected that the estimation of the transition point will be less successful. Nevertheless, because of the lack of anything better, an attempt is made to obtain an approximate variation of transition Reynolds number with Mach number. The assumptions involved in the calculation are as follows: (1) the amplification ratio at breakdown is the same as in the incompressible case ($\log[\tilde{Q}/Q_0] = 6{\cdot}5$, which yields the transition Reynolds number $R_x = 3 \times 10^6$ observed by Schubauer & Skramstad); (2) the initial amplitude

Q_0 of the critical disturbances is independent of frequency and Mach number; (3) the ratio c/c_{inc} is independent of R_δ.

From the form of the disturbance (3.1) we may write

$$\log\frac{\tilde{Q}}{Q_0} = \int_{t(x_0)}^{t(x)} \beta_i\, dt = \int_{x_0}^{x} \frac{\beta_i}{c}\, dx$$

$$= \frac{2}{a^2}\int_{R_{\delta_0}}^{R_\delta} \frac{\overline{U}_1}{c}\frac{\beta_i \delta}{\overline{U}_1}\, dR_\delta \quad \text{since} \quad \frac{\delta}{x} = \frac{a}{\sqrt{R_x}},$$

where a is constant.

In the incompressible case, Pretsch calculated and charted the value of this integral for all unstable frequencies. By means of his calculations,* it is easily verified that the minimum Reynolds number at which the disturbance reaches an amplification ratio $\log(\tilde{Q}/Q_0) = 6{\cdot}5$ turns out to be $R_\delta = 10{,}400$ or $R_x = 3 \times 10^6$. For the compressible case on the basis of assumption 3, one may rewrite the above equation

$$\log\frac{\tilde{Q}}{Q_0} = 6{\cdot}5 = \left[\frac{a_{\text{inc}}^2}{a^2}\frac{c_{\text{inc}}}{c}\right]\left[\frac{2}{a_{\text{inc}}^2}\int_{R_{\delta_0}}^{R_{\delta_{\text{tr}}}} \frac{\overline{U}_1}{c_{\text{inc}}}\frac{\beta_i \delta}{\overline{U}_1}\, dR_\delta\right].$$

Using the present experimental result that $\beta_i \delta/U_1$ is a function of R_δ only, independently of M, Pretsch's charts can be used for the evaluation of the second factor on the right-hand side of the above equation. The new 'fictitious' amplification ratio is

$$\frac{a^2}{a_{\text{inc}}^2}\frac{c}{c_{\text{inc}}}\,6{\cdot}5.$$

The table below shows the transition Reynolds number ratios for various Mach numbers and the approximate values of c/c_{inc} used in the calculation:

M	0	0·4	0·8	1·3	1·6	2·0
c/c_{inc}	1·0	1·06	1·13	1·20	1·33	1·76
$[R_x/R_{x,\text{inc}}]_{\text{tr}}$	1·0	1·1	1·2	1·4	1·6	2·3

The rapid increase in transition Reynolds number is quite apparent.

6. Conclusion

A detailed exploration has been made of small-amplitude disturbances in a laminar supersonic layer up to $M = 2{\cdot}2$, and the stability of the layer with respect to these perturbations was examined. The results may be summarized as follows.

(1) The experiments succeeded in detecting self-excited oscillations in the layer. Generally speaking, the basic features of these oscillations are the same as found in the incompressible layer and are in agreement with the existing theory. Specifically, the boundary layer acts as a frequency selective-amplifier with respect to the disturbances: depending on the local Reynolds number, it attenuates certain frequencies and amplifies others, thus causing detectable oscillations in a narrow bandwidth.

(2) Amplitude distributions of velocity, temperature, and density fluctuations have been calculated from the measurements. It was found that at $M = 2{\cdot}2$

* The authors are grateful to A. M. O. Smith, who extended and re-plotted Pretsch's calculations in a more convenient form and made his charts accessible.

the temperature and density fluctuations are several times that of the velocity, and this ratio is shown to increase further with increasing Mach number.

(3) Comparing the results with the stability theory of Lees, Lin, and Dunn, one may conclude that the theory predicts correctly the basic features of the compressible-boundary-layer stability. Quantitatively, the viscous solutions predict Reynolds numbers corresponding to the lower stability limits which are considerably below the measured values. On the other hand, the theoretical upper stability branch agrees very well with that obtained by the experiments.

(4) Within the accuracy of the measurements, results of the incompressible and compressible stability problem may be correlated; it is shown that up to $M = 2{\cdot}2$ the stability limits (two positions on the plate between which a disturbance is amplified) of a perturbation of a given frequency depend only on the Reynolds number based on the local boundary-layer thickness δ, and are independent of the Mach number. Furthermore, the non-dimensional amplification coefficient $\delta\beta_i/\overline{U}_1$ depends only on the local eigenvalues (frequency, R_δ) and not on the Mach number.

(5) The effect of compressibility manifests itself mainly in changing the wave velocity of the disturbances: they propagate faster with increasing Mach number. This has the important consequence that a disturbance propagating to a given x-position will not be amplified as much in a higher Mach number flow because its time available to grow is less, even though its amplification coefficient $(\delta\beta_i/\overline{U}_1)(R_\delta)$ is the same. Thus, the adiabatic compressible boundary layer is shown to be more stable with respect to small disturbances than the incompressible one.

(6) On the basis of the above results, a rough estimate of the transition Reynolds number is made; the calculations indicate a considerable increase in its value as the Mach number increases.

The authors wish to acknowledge the constant support and encouragement of Drs F. E. Goddard and P. P. Wegener of the Jet Propulsion Laboratory during the entire period of this investigation. The extremely valuable discussions with Prof. Lester Lees, Drs Leslie M. Mack, Alan Kistler, Eli Reshotko, and R. Betchov are also gratefully acknowledged. Mr Carl Thiele contributed many basic ideas in the design of the mechanical and electronic systems used, while Mr A. Irving and his group and Mr W. Simms carried out their construction expertly. Their valuable help contributed greatly to the results of the investigation.

This paper presents the results of one phase of research carried out at the Jet Propulsion Laboratory, California Institute of Technology, under joint sponsorship of the Department of the Army, Ordnance Corps (under Contract No. DA-04-495-Ord 18), and the Department of the Air Force.

Notation

c	wave velocity
C_v	specific heat at constant volume
e	hot-wire voltage
e_f	hot-wire voltage filtered by wave analyser

Δe a dimensionless hot-wire voltage fluctuation
f frequency
i heated-wire current
k thermal conductivity
m mass flow
M Mach number
p static pressure
Re Reynolds number
R_r unheated-wire resistance
R_w heated-wire resistance
R_θ Reynolds number based on boundary-layer momentum thickness
R_δ Reynolds number based on boundary-layer thickness at $u/\overline{U}_1 = 0{\cdot}999$
Q' perturbation of any one of the flow quantities
S hot-wire sensitivity factor
t time
T static temperature
u velocity in the x-direction
$\overline{U}_1$ mean velocity in free stream
v' velocity fluctuation perpendicular to plate
x co-ordinate along the free-stream direction; $x = 0$ corresponds to plate leading edge
y co-ordinate perpendicular to free-stream direction and the flat plate; $y = 0$ corresponds to plate surface
X, Y abscissa and ordinate on the plotting table
α wave-number
β $2\pi f$, angular frequency
β_i damping coefficient
γ ratio of specific heats
$\Gamma = \int_0^1 \tilde{e}_f d\frac{y}{\delta}$
δ boundary-layer thickness
θ boundary-layer momentum thickness
λ $2\pi/\alpha$, wavelength
μ viscosity
ν kinematic viscosity
ρ density

Superscripts and subscripts

$\overline{(\ )}$ temporal mean
$\overline{(\ )}^2$ mean-square value of a fluctuating quantity
$\widetilde{(\ )}$ root-mean-square value of a fluctuating quantity
$(\ )'$ instantaneous value of a fluctuating quantity
$(\ )_1$ free-stream condition
$(\ )_T$ stagnation condition

REFERENCES

BENNET, H. W. 1953 *An Experimental Study of Boundary Layer Transition.* Neenah, Wisconsin: Kimberly-Clark.

DEMETRIADES, A. 1958 An experimental investigation of the stability of the hypersonic laminar boundary layer. *J. Aero./Space Sci.* **25**, 599.

DEMETRIADES, A. 1960 An experiment on the stability of the hypersonic laminar boundary layer. *J. Fluid Mech.* **7**, 385.

DRYDEN, H. L. 1955 Transition from laminar to turbulent flow at subsonic and supersonic speeds. *Proceedings of the Conference on High-Speed Aeronautics*, no. 41. Polytechnic Institute of Brooklyn.

DUNN, D. W. & LIN, C. C. 1955 On the stability of the laminar boundary layer in a compressible fluid. *J. Aero. Sci.* **22**, 455.

KLEBANOFF, P. S. & TIDSTROM, K. D. 1959 Evolution of amplified waves leading to transition in a boundary layer with zero pressure gradient. *N.A.S.A. Tech. Note*, no. D-195.

KOVASZNAY, L. S. G. 1953 Turbulence in supersonic flow. *J. Aero. Sci.* **20**, 657.

KOVASZNAY, L. S. G. 1954 Development of turbulence-measuring equipment. *N.A.S.A. Rep.* no. 1209.

LAUFER, J. 1956 Experimental observation of laminar boundary-layer oscillations in supersonic flow. *J. Aero. Sci.* **23**, 184.

LAUFER, J. 1959 Aerodynamic noise in supersonic wind tunnels. Jet Propulsion Laboratory, Pasadena, California, Progress Rep. no. 20–378.

LAUFER, J. & MCCLELLAN, R. 1956 Measurement of heat transfer from fine wires in supersonic flows. *J. Fluid Mech.* **1**, 276.

LAUFER, J. & VREBALOVICH, T. 1957 Experiments on the instability of a supersonic boundary layer. IX. Congrès International de Mécanique Appliquée, Université de Bruxelles.

LAUFER, J. & VREBALOVICH, T. 1958 Stability of a supersonic laminar boundary layer on a flat plate. Jet Propulsion Laboratory, Pasadena, California, Rep. no. 20–116.

LEES, L. 1947 The stability of the laminar boundary in a compressible fluid. *N.A.C.A. Rep.* no. 876.

LEES, L. 1952 Instability of laminar flows and transition to turbulence. Consolidated Vultee Aircraft Corporation, San Diego, California, Rep. no. ZA-7-006.

LEES, L. & LIN, C. C. 1946 Investigation of the stability of the laminar boundary layer in a compressible fluid. *N.A.C.A. Tech. Note*, no. 1115.

LIEPMANN, H. W. 1943 Investigations on laminar boundary-layer stability and transition on curved boundaries. *N.A.C.A. Rep.* no. W-107.

LIEPMANN, H. W. & ROSHKO, A. 1957 *Elements of Gasdynamics.* New York: John Wiley and Sons.

LIN, C. C. 1945 On the stability of two-dimensional parallel flows. *Quart. Appl. Math.* **2**, 117; **3**, 218; **4**, 277.

LIN, C. C. 1958 On the instability of laminar flow and its transition to turbulence. *IUTAM Symposium on Boundary Layer Research at Freiburg, 1957*, pp. 144–87. Springer.

MACK, L. M. 1958 Calculation of the laminary boundary layer on an insulated flat plate by the Klunker–McLean method. Jet Propulsion Laboratory, Pasadena, California, Progress Rep. no. 20–352.

MACK, L. M. 1960 Numerical calculation of the stability of the compressible laminar boundary layer. Jet Propulsion Laboratory, Pasadena, California, Rep. no. 20–122.

MORKOVIN, M. V. 1956 Fluctuations and hot-wire anemometry in compressible flows. North Atlantic Treaty Organization, Advisory Group for Aeronautical Research and Development, Paris, AGARDograph 24.

MORKOVIN, M. V. 1958 Transition from laminar to turbulent shear flow—a review of some recent advances in its understanding. *Trans. Amer. Soc. Mech. Engrs*, **80**, 1121.

SCHUBAUER, G. B. 1958 Mechanism of transition at subsonic speeds. *IUTAM Symposium on Boundary Layer Research at Freiburg, 1957*, pp. 85–107. Springer.

SCHUBAUER, G. B. & SKRAMSTAD, H. K. 1948 Laminary-boundary-layer oscillations and transition on a flat plate. *N.A.C.A. Rep.* no. 909.

SMITH, A. M. O. 1956 Transition, pressure gradient and stability theory. Douglas Aircraft Rep. no. ES 26388.

STRONG, J. 1938 *Procedures in Experimental Physics*, p. 134. Englewood Cliffs, New Jersey: Prentice-Hall.

TOLLMIEN, W. 1929 Über die Entstehung der Turbulenz. *Nachrichten der Gesellschaft der Wissenschaften zu Göttingen, Mathematisch-Physikalische Klasse*, pp. 21–44. (Translated as *N.A.C.A. Tech. Memo.* no. 609.)

TUCKER, M. 1953 Combined effect of damping screens and stream convergence on turbulence. *N.A.C.A. Tech. Note*, no. 2878.

WORTMANN, F. X. 1955 Untersuchung instabiler Grenzschichtschwingungen in einem Wasserkanal mit der Tellurmethode. *50 Jahre Grenzschichtforschung*, pp. 460–70. Braunschweig: Friedr. Vieweg und Sohn.